IMPACT INDUCED PROPAGATION OF PHASE TRANSFORMATION IN A SHAPE MEMORY ALLOY ROD

A. BEKKER, J. C. JIMENEZ-VICTORY, P. POPOV, D. C. LAGOUDAS
Aerospace Eng. Dept., Texas A&M University
College Station, TX 77843 - 3141

ABSTRACT

In this work we study the propagation of a phase-transformation front induced by an impact loading. Our main goals in this paper are to demonstrate the wave structure of the solution to the impact loading and to estimate the velocity of phase front propagation using a thermodynamically based constitutive model for SMAs with internal variables. First, we study the impact problem in an isothermal setting; this study provides an important insight into the wave structure of the solution. The non-uniqueness issue inherent to such problems due to nonconvex SMA constitutive models is thoroughly discussed. Then we develop the solution for an adiabatic approximation for a simplified SMA model. Several numerical examples based on a first order Lax-Friedrichs finite difference scheme are presented.

1. INTRODUCTION

A polycrystalline Shape Memory Alloy (SMA) body subjected to external impact loading will experience deformations that will propagate along the SMA body as stress waves. Loading that produces stresses below the critical values for stress-induced phase transformation generates only elastic waves. Impact loading that results in stresses less than the SMA plastic yield limit but above the critical stresses for stress-induced phase

transformation generates phase transformation waves in addition to the purely elastic waves.

Extensive study of 1-D dynamic phase front propagation in materials with transformation softening behavior has been conducted by James [7], Pence [8], Abeyaratne and Knowles [9, 10, 11, 55] and Truskinovsky [12, 13]. The non-uniqueness issue inherent in the Riemann problem for such materials has been thoroughly discussed. In these studies, the phase front is represented by a jump discontinuity separating the different austenite (A) and martensite (M) branches of the *N*-shaped stress-strain curve. In contrast to the present work the constitutive models employed by the above authors are rate dependent and include an additional constitutive assumption about a *driving force* [9, 10, 11] that establishes the speed of the transformation front. In the papers mentioned above, a 1-D analysis of the phase front propagation is carried under the assumption that the change in cross-sectional area of the 1-D body can be neglected. Changes in density can then be post-calculated using the already computed strain field, as Abeyaratne and Knowles [11] did. A new approach on defining driving force in inelastic materials is proposed by Levitas [66].

The main focus of this article is the construction of the wave structure of the solution to the impact loading problem for a 1-D SMA body and the determination of the velocity of phase front propagation. An extensive study on the uniqueness problem is also performed. The SMA materials of consideration have transformation hardening behavior and are modeled by a phenomenological rate independent macro-constitutive law with an internal state variable, the martensite volume fraction as developed by Tanaka [1, 2], Bekker [3], Bekker and Brinson [4, 5] and Boyd and Lagoudas [6]. Recently there have been numerous developments in SMA constitutive modeling. The early phenomenological rate independent models [1-6] have been unified in a constitutive model [23] based on the selection of appropriate thermodynamic potentials. A recent work by Chen and Lagoudas [44] explored an impact problem similar to the one

discussed in this paper but using the unified model [23]. In a further development of the model, Qidwai and Lagoudas [57] extended it by incorporating the principle of maximum transformation dissipation. They also generalize the transformation surfaces in order to capture the tension/compression asymmetry observed in the mechanical behavior of most SMAs.

There has also been extensive research on constitutive models based on micromechanics. In the works of Patoor et al., [64]; Sun and Hwang [26]; Tokuda et al. [65] the macroscopic response of a polycrystalline SMAs is derived by modeling single crystals and averaging their response over a representative volume element. In more recent developments, Gao Hunag and Brinson [58,59], building on a previous work [62] developed a mutlivariant model based on micromechanics of martensitic variants. The model takes into account the stress induced phase transformation as well as the detwinning of martensite. Sittner and Novak [60] present a theoretical study on the effects of single crystal orientations in a polycrystalline CuAlNi SMAs on the macroscopic compression/tension asymmetry. Gall et al. [62] study the effects of grain boundaries on the macroscopic properties of polycrystalline NiTi SMAs with the help of a micromechanical finite element model. A similar numerical tool is used by Kitajima et al. [63] to simulate the micromechanical behavior of the different martensitic variants in complex thermomechanical loads.

After a brief introduction to the SMA constitutive model in Section 2, the mathematical model for the impact problem is presented in Section 3. The incompressibility constrained is incorporated into the 1-D field equations and the isothermal and adiabatic approximations are developed. The solution to the initial boundary value problem under isothermal conditions is formulated in Section 4.1. Section 4.2 establishes the wave structure of the solution to the impact problem for SMA materials with transformation hardening behavior and presents a detailed analysis on the uniqueness of the solution. The study of the isothermal approximation is concluded by

two numerical examples in section 4.3 using a finite difference scheme. The adiabatic case is finally investigated in section 5. For a detailed discussion of the constitutive model, the isothermal approximation with various other cases such as convex, concave and bilinear isotherms the reader is referred to [56].

2. SMA CONSTITUTIVE MODEL

Our constitutive model is based on a 1-D, rate-independent constitutive law [2, 5] of the form

$$s = \mathrm{E}e + \Theta\left(T - T_0\right) + \Omega x^d \tag{2.1}$$

or

$$e = e^{EL} + e^{TH} + e^{TR} = \mathrm{K}s + a\left(T - T_0\right) + \Lambda x^d, \tag{2.2}$$

where s is the uniaxial stress, T is the temperature, e^{EL} is the elastic strain, e^{TH} is the thermal strain, and e^{TR} is the transformation strain. The Young's modulus is given by E, while Ω and Θ are the transformation and thermoelastic coefficients of the 1-D SMA body. For simplicity $\mathrm{K} = \mathrm{E}^{-1}$ (elastic compliance), $a = -\Theta\mathrm{E}^{-1}$ (thermal expansion coefficient), and $|\Lambda| = |\Omega\mathrm{E}^{-1}|$ (maximum transformation strain) are assumed to be constant. Note that $\Lambda > 0$ for tensile and $\Lambda < 0$ for compressive loading.

The variable x^d $(0 \le x^d \le 0)$ represents the volume fraction of the material transformed to a detwinned martensitic state and serves as the internal state variable in the constitutive law (2.1). Due to the diffusionless character of the stress-induced phase transformation on a macroscopic level, x^d is determined by the current values of temperature and stress, T and s, and prior loading history. In this work, we employ the kinetic law previously developed in [3], [4] and [5], which is essentially based on the experimentally defined s - T phase diagram shown in Figure 1. In [3], [4] and [5], the phase diagram shown was described in detail. Here we present only the features necessary for the present study. The phase diagram is divided by the transformation strips **[A]**, **[M]**, **[d]** and **[t]** into the four major regions **A**, $\mathbf{M^d}$, $\mathbf{M^{t,d}}$ and $\mathbf{M^{t,d}A}$. In region **A**,

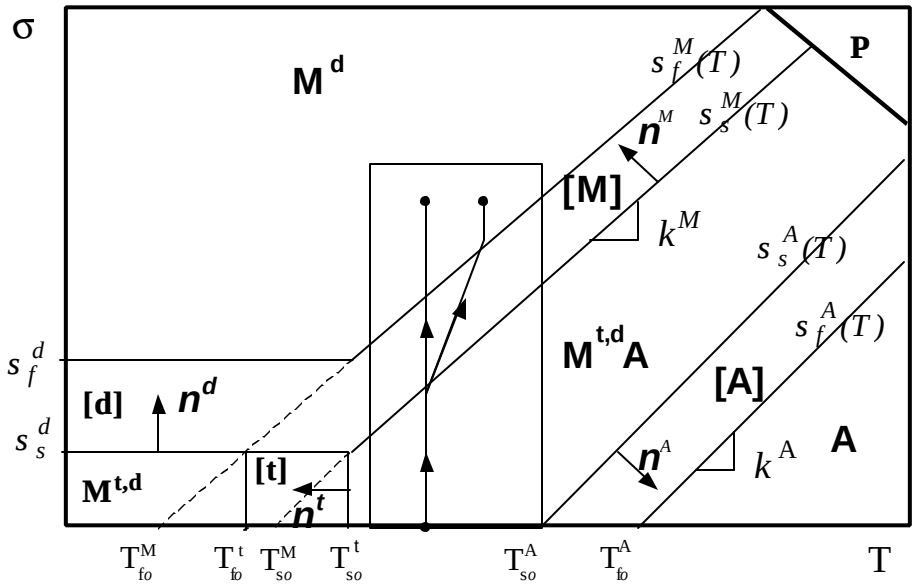

Figure 1. Shape memory alloy stress-temperature phase diagram

only austenite can exist. In region $\mathbf{M^d}$, only detwinned martensite can exist. In region $\mathbf{M^{t,d}}$, both twinned and detwinned martensite can exist. In region $\mathbf{M^{t,d}A}$, all phases can coexist. Transformation from one phase to another occurs in the strips when a point (T, s) representing a local state of the 1-D SMA moves across a strip in the direction indicated by the *director vectors* $n^i = (n_1^i, n_2^i)$ (i = **A**, **M**, **d**) in the phase diagram. Note that the transformation regions (strips) are bounded by the parallel lines $s = s_S^i(T)$ and $s = s_f^i(T)$ (i =A, M, d) (start and finish boundaries). Similarly, we define the start and finish critical temperatures $T_S^i(s)$ and $T_f^i(s)$, i =**A**, **M**, which are the inverse functions to the critical stress functions. For convenience, we introduce the following temperatures:

$$\begin{aligned} T_{S0}^M &= T_S^M(0) = T_{S0}^t - s_S^M(T_{S0}^t)/k^M \\ T_{f0}^M &= T_f^M(0) = T_{f0}^t - s_f^M(T_{f0}^t)/k^M \end{aligned} \tag{2.3}$$

where $k^M = -n_1^M / n_2^M$. Then the equations of the start and finish boundaries $s_S^M(T)$ and $s_f^M(T)$ of strip **[M]** can be expressed as $s_j^M(T) = k^M(T - T_{j0}^M)$, $j = S, f$.

The presence of the coexistence regions and transformation strips on the phase diagram makes it clear that the transformation state of an SMA material is path-

dependent. In this paper, we focus on SMA behavior in the subregion of the phase diagram (Figure 2) where the stress induced phase transformation follows the path $a \to b$ (isothermal loading) or $a \to c$ (adiabatic loading). Since the transformation process considered in this paper is always from austenite to a detwinned martensite (i.e., forward from A to M^d), we will drop the superscript d from now on; for example, we will write $A \to M$ and x instead of $A \to M^d$ and x^d.

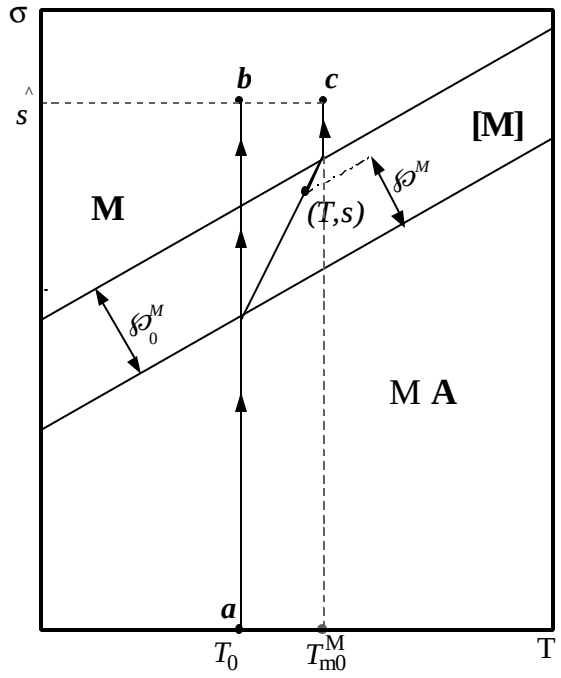

Figure 2: Magnified region of the stress-temperature diagram representing the thermomechanical loading paths of interest.

Due to the simplicity of the thermomechanical loading 'paths' for the impact problem, the global kinetic law for the volume fraction of martensite may be written simply as [4, 5]

$$x = \Xi(T, s) = \begin{cases} 0, & if \ \ (T, s) \in \mathbf{MA} \\ F^M(T, s), & if \ \ (T, s) \in [\mathbf{M}], \\ 1, & if \ \ (T, s) \in \mathbf{M} \end{cases} \tag{2.4}$$

where $F^M(T,s) = f^M\left(Z^M(T,s)\right)$. The function $F^M = f^M \circ Z^M$ is a local kinetics law (*M*-branch) that represents the change in the phase fraction across the strip **[M]**, f^M is the *M*-transformation function, and $Z^M(T,s)$ is the normalized distance from a point $(T,s) \subset [\mathbf{M}]$ to the start boundary of the **[M]** strip given by

$$Z^M(T,s) = \frac{\wp^M(T,s)}{\wp_0^M}, \tag{2.5}$$

where $\wp^M = k^M(T - T_{S0}^M) - s$, $\wp_0^M = k^M(T_{f0}^M - T_{S0}^M)$ and the normalized distance Z^M is a linear function of T and s:

$$Z^M(T,s) = a^M(T - T_S^M(s)) = a^M(T - T_{S0}^M) + b^M s$$

$$T_S^M(s) = T_{S0}^M + s/k^M,\ a^M = 1/(T_{f0}^M - T_{S0}^M),\ b^M = -a^M/k^M.$$

In the first approximation, one can assume that the phase diagram for compressive loading is symmetric to the tensile phase diagram with respect to the *T*-axis [4] (see Figure 1), so that $k^M \to -k^M$ when $s \to -s$, and therefore

$$\Xi(s,T) \underset{k^M \to -k^M}{=} \Xi(-s,T). \tag{2.6}$$

So the kinetic law (2.4) is invariant under the transformation $s \to -s$, $k^M \to -k^M$.

The most popular transformation functions (kinetics) are:

Linear function

$$f^M(Z^M) = Z^M \tag{2.7}$$

Exponential function

$$f^M(Z^M) = 1 - \exp(gZ^M),\ g = \ln 0.01 \tag{2.8}$$

Cosine function

$$f^M(Z^M) = \frac{1}{2}\left\{1 - \cos(pZ^M)\right\} \tag{2.9}$$

Any of the kinetic laws (2.7-9) can be viewed as a particular case in the framework of a constitutive model based on thermodynamics [23]. It has been shown there that these three kinetic laws can be obtained by specific selection for the form of the Gibbs free energy.

3. FIELD EQUATIONS

We consider the boundary value problem of the tensile impact loading of a 1-D, semi-infinite SMA rod that is initially in an austenitic phase and that has uniform cross-sectional area A_0 and temperature T_0. The rod occupies the positive part if the real axis $x \in [0, \infty)$ and the boundary $x = 0$ is subjected to the tensile shock loading

$$s(0,t) = \hat{s}\, H(t) \quad \text{for} \quad t > 0 \tag{3.1}$$

where $H(t)$ is the Heaviside function and $\hat{s} > 0$ is below the plastic yield limit of the material s_Y but higher than the critical transformation stress $s_f^M = s_f^M(T_0)$ for the initial temperature T_0: $s_Y > \hat{s} > s_f^M$.

For a one-dimensional rod approximation we assume uniaxial displacement $u(x,t)$, strain $e(x,t)$, stress $s(x,t)$ and temperature $T(x,t)$. Initially the rod has a uniform cross-section A_0 but due to lateral deformations it will become a nonuniform function $A(x,t)$. All field variables are assumed averaged over the cross-section of the rod. Since we consider fast processes associated with impact induced wave propagation, we ignore heat transfer through the lateral surface of the rod. In this paper we assume infinite small strain $e = u_x(x,t)$ [1]. The conservation of mass, linear momentum and energy read (e.g. [53],[54]):

$$\begin{aligned} A_t &= -Ae_t \\ \rho A u_{tt} &= (sA)_x \\ \rho A U_t &= sAe_t + k_0 (AT_x)_x \end{aligned} \tag{3.2}$$

where $U(x,t)$ is the internal energy per unit mass. The continuity equation can be integrated to yield $A = A_0 e^{-e}$. Then we can write the dynamic equation of motion and the conservation of energy in the form:

$$\rho u_{tt} = s_x - se_x \tag{3.3}$$

$$\rho U_t = se_t + k_0 T_{xx} - k_0 e_x T_x \tag{3.4}$$

[1] Here a subscript indicates a partial derivative, i.e. $u_x = \dfrac{\partial u}{\partial x}$, $u_t = \dfrac{\partial u}{\partial t}$, etc.

Here we consider the density r and thermal conductivity k_0 to be constant[2] along the length of the rod.

In this paper we consider only the isothermal and adiabatic approximations to the system of equations (3.3) and (3.4) for the reasons explained below.

In the *isothermal case*, the temperature is constant ($T = T_0$), and one only needs to consider the balance of linear momentum (3.3) where $s = s(e, T_0)$ is the isothermal stress-strain relationship for SMAs. The isothermal condition is not realizable for fast-moving phase front propagation unless the latent heat of the transformation is very small. The isothermal solution will serve as a natural starting point that provides an important insight to the wave structure of the solution of the impact loading problem, which later will be used for the adiabatic case.

In the *adiabatic approximation* heat conduction is disregarded and the energy equation in (3.4) takes the form

$$r U_t = s e_t . \tag{3.5}$$

We want to express this equation in terms of the entropy S. For this purpose we need to introduce the Gibbs free energy $G = G(s, T, x)$. We have

$$S = -\frac{\partial G}{\partial T}, e = -r \frac{\partial G}{\partial s}, p = -r \frac{\partial G}{\partial x} \tag{3.6}$$

where S is the entropy and p is the driving force for the transformation. Now, using a standard Legendre transform $U = G + TS + r^{-1} s e$ one rewrites (3.5) as:

$$r T S_t = p x_t \tag{3.7}$$

Further, the particular form of the entropy for SMA materials given in [23] is:

$$S = a s / r + C \ln(T/T_R) - \Delta S_R x + S_R^A \tag{3.8}$$

where C is the heat capacity (assumed equal for Austenite and Martensite) and $\Delta S_R = S_R^A - S_R^M$ is the difference in entropies of the two phases (in the reference state). The reference temperature is denoted by T_R. Substituting (3.8) in (3.7) on finds that

[2] The martensitic phase transition is essentially volume conserving which justifies the assumption that r is constant.

$$r C T_t = -a T s_t + (p + r\Delta S_R T) x_t, \tag{3.9}$$

According to [27] and [28] $p \ll r\Delta S_R T$ for most SMAs (e.g. for NiTi the precise values yield $p / r\Delta S_R T < 1.3\%$) so we can approximate (3.9) by

$$r C T_t = -a T s_t + r\Delta S_R T x_t, \tag{3.10}$$

which is equivalent to the isentropic condition

$$S_t = 0. \tag{3.11}$$

Furthermore, if we compare the two heat sources ($aTs_t = (a s_Y) T z_t$, $z = s / s_Y < 1$ due to thermoelasticity and $(rDS_R) T x_t$ due to phase transformation), it becomes clear that the thermoelastic heat-generation term can be disregarded, since $a s_Y \ll r\Delta S_R$ (typically for NiTi-based SMA, $a = 6.10^{-6}\,1/\mathrm{K}$, $s_Y = 600$ MPa and $r\Delta S_R = 0.46$ MJ/m^{3}K). Therefore, Equation (3.10) reduces further to

$$C T_t = \Delta S_R T x_t \tag{3.12}$$

and the temperature changes only due to the phase transformation; that is, it is enslaved to the martensitic volume fraction x. Equation (3.12) can be integrated to yield

$$T = T_0 \exp(w x), \tag{3.13}$$

where $w = D S_R / C$ and $T\big|_{x=0} = T_0$. Thus, the maximum attainable temperature due to the phase transformation is given by

$$T_{\mathrm{m0}}^M = T\big|_{x=1} = T_0 \exp(w). \tag{3.14}$$

4. ISOTHERMAL CASE

4.1 Solution development. For isothermal loading paths the field equation (3.3) is complemented by the constitutive and kinetic law (2.2) and (2.4). For a constant temperature $T = T_0$ they take the form

$$\begin{aligned} e &= \mathrm{K} s + \Lambda x \\ x &= \Xi(T_0, s) \end{aligned} \tag{4.1}$$

and define the isotherm $e = I(T_0, s) = \mathrm{K} s + \Lambda \Xi(T_0, s)$. As we stated before, we will concentrate here on the tensile loading case: s, $e, L > 0$. By definition, an isotherm for

SMA materials with transformation hardening behavior is a monotone increasing function of s , and therefore the inverse function $s = s(e) = I^{-1}\{T_0, e\}$ is also monotone increasing. The momentum equation (3.3) can be rewritten as

$$r u_{tt} = \big(s'(e) - s(e)\big) e_x = f'(u_x) u_{xx} \tag{4.2}$$

where

$$f'(e) = s'(e) - s(e) \tag{4.3}$$

$$f(e) = s(e) - \int_o^e s(e)de \cong s(e) - e s(e). \tag{4.4}$$

The second term in the right hand side of (4.3), (4.4) represents the geometrical softening effect due to the change in cross-sectional area of the rod during transformation and is negligible for small strains $e < 1\%$, so that $f'(e) \cong s'(e)$, $f(e) \cong s(e)$. For our case $e < \Lambda \cong 0.05$. However, for SMA materials with very large transformation strains ($\Lambda \geq 0.1$), these terms can become significant.

As we stated above, we consider SMA materials with transformation hardening behavior; that is, with monotone increasing isotherms $s(e)$ such that $s' > 0$. We further restrict the class of materials even more, and from now on we will only consider SMA materials with **strong** hardening transformation behavior and with monotone increasing $f(e)$ that is, $f'(e) > 0$. This ensures that all initial boundary value problems that will be considered are hyperbolic and well posed.

Finally, due to the symmetry of the isotherm if one disregards the change in the cross-sectional area of the rod all results obtained below for tensile loading are equally applicable to tensile loading.

Shock loading problem. We can rewrite the original wave equation (4.2) as a first order hyperbolic system

$$\begin{aligned} e_t &= \mathrm{v}_x \\ r\mathrm{v}_t &= f_x \end{aligned} \tag{4.5}$$

This system, together with the initial

$$\begin{aligned} e &= u_x(x,0) = 0 \\ \mathrm{v} &= u_t(x,0) = 0 \end{aligned} \tag{4.6}$$

and boundary conditions

$$e(0,t) = \hat{e}H(t), \quad t \geq 0, \tag{4.7}$$

define the isothermal impact problem. Here (4.7) is nothing else but the boundary condition (3.1) expressed in terms of the stress:

$$\hat{s} = s(\hat{e}) = I^{-1}(T_0, \hat{e}) \tag{4.8}$$

The acoustic velocity is clearly

$$c(e) = \sqrt{\frac{f'(e)}{r}} = \sqrt{\frac{s'(e) - s(e)}{r}} \tag{4.9}$$

with real characteristic curves given by

$$\begin{aligned} \mathbf{C}^+ &: \dot{x} = c(e) \\ \mathbf{C}^- &: \dot{x} = -c(e). \end{aligned} \tag{4.10}$$

We can reject left-going waves and integrate the first of these equations to yield

$$\mathbf{C}^+ : x = c(e)t + const = c(e)(t - t). \tag{4.11}$$

The characteristics $\mathbf{C}^+$ are a family of straight lines and the parameter t is the time at which the line (4.11) intersects the Ot axis. The slope of this line is determined by the boundary condition $e = e(0,t) = \mathrm{E}(t)$.

Two types of discontinuities can develop as the wave propagates in the rod. One is due to the shock character of the boundary condition (4.7a). The other is due to the convex-concave structure of the function $f(e)$. The later are true nonlinear shock that develop because of increasing wave velocity as the strain e increases and reaches the region where $f(e)$ is convex down, that is $f''(e) > 0$. For a stress-strain discontinuity $\mathbf{S}$ with trajectory $x = s(t)$ we need the Rankine-Hugoniot jump conditions (see e.g., [51]):

$$\begin{aligned} D(e_- - e_+) + (\mathrm{v}_- - \mathrm{v}_+) &= 0 \\ r\,D(\mathrm{v}_- - \mathrm{v}_+) + (f_- - f_+) &= 0, \end{aligned} \tag{4.12}$$

where $D = \dot{s}(t)$ is the velocity of the shock, $f_{\pm} = f\{s(t) \pm 0\}$ and $f = \mathrm{v}, e, f$. From (4.12), we obtain

$$D = \sqrt{\frac{f_- - f_+}{r(e_- - e_+)}} \tag{4.13}$$

for forward-moving discontinuities $\bar{\mathbf{S}}$.

It is easy to see that when the amplitude of a shock wave is very small ($e_- \to e_+ = e$) and that the velocity of the shock reduces to the acoustic velocity ($D \to \sqrt{f'(e)/r}$) at the points where $f(e)$ is differentiable.

The solution procedure given below is essentially based on the one employed by Barenblatt [32] for the impact loading problem for a half-space with a nonlinear elastic material. As in [32], we introduce the dimensionalized function

$$\Phi(e) = f(e)/rV^2.$$

where V is a characteristic velocity. Then Equation (4.2) takes the form

$$u_{tt} = V^2 \Phi'(u_x) u_{xx}. \tag{4.14}$$

Since the formulation of our problem given in Equations (4.2), (4.6) and (4.7) contains no characteristic time or length scales, it follows from the dimensional analysis [33] that a solution of the problem must have the form

$$\frac{u}{Vt} = f\left(\frac{x}{Vt}\right).$$

Let us denote $z = \dfrac{x}{Vt}$ and $g = f'$. The field variables for the above solution take the form $e = g(z)$, $s = s\left(g(z)\right)$ and $\mathrm{v} = Vf(z) - Vz\,g(z)$ and upon substitution into (4.14), we obtain

$$g'\left(z^2 - \Phi'(g)\right) = 0. \tag{4.15}$$

Equation (4.15) for a monotone increasing function Φ with $\Phi' > 0$ admits two types of continuous solutions $e = g(z)$ that satisfy the equations

$$\begin{aligned} g' &= 0 \\ z^2 - \Phi'(g) &= 0 \end{aligned} \tag{4.16}$$

correspondingly. These solutions are constant state **C** and centered simple wave (centered fan) **F**:

$$\begin{aligned} &\mathbf{C}: \ e = const \\ &\mathbf{F}: \ e = l(z) := (\Phi')^{-1}(z^2). \end{aligned} \tag{4.17}$$

Therefore, a solution of the shock loading problem for a monotone increasing function $f(e)$ is a combination (nonlinear superposition) of these two elementary solutions.

Before we turn our attention to SMA materials with a nonconvex function $f(e)$, we briefly review the results [32] for the cases where the function $f(e)$ is strictly convex up or convex down.

4.2. Analytical Results

4.2.1 Smooth isotherms. First, we consider the shock loading problem for an SMA material with cubic-like convex-concave function $f(e)$ (i.e. one that has a single inflection point). Let us denote by $\bar{e}$ the inflection point of the function $f(e)$, and by $\tilde{e}$ the point (other than the origin) where the line that is tangent to the curve $f(e)$ at the origin again intersects the curve $f(e)$ (that is, such that $f'(0)\tilde{e} = f(\tilde{e})$). Note that $\bar{e} < \tilde{e}$. We consider only low-intensity impact loading with relatively small amplitude $\hat{e}$ for which $\hat{e} \le \tilde{e}$. In this case, all shocks in the SMA material are weak (underdriven) and, as we shall see later, are either linear elastic shocks or phase transformation fronts.

If the shock loading amplitude $\hat{e}$ is such that $\hat{e} \le \bar{e}$, then waves emitted from the left end will propagate with continually decreasing velocities. The solution will resolve in a centered fan $\bar{\mathbf{F}}$. The front of the centered fan propagates into the undisturbed region of the rod with speed $c_0 = V\sqrt{\Phi'(0)}$, so that $e = l(z_0) = 0$ where $z_0 = c_0/V = \sqrt{\Phi'(0)}$. The tail (last characteristic, $\mathbf{C}^+$) of the fan $\bar{\mathbf{F}}$ has speed $\hat{c} = V\sqrt{\Phi'(\hat{e})}$, so that $e = l(\hat{z}) = \hat{e}$, where $\hat{z} = \hat{c}/V = \sqrt{\Phi'(\hat{e})}$. The solution can be written

$$\begin{aligned} e &= \hat{e}L(z) \\ s &= s\left(\hat{e}L(z)\right) \\ v &= \hat{e}V'L(z) - \hat{e}Vz\,L(z), \end{aligned}$$

where

$$L(z)=\begin{cases}1 & \text{if } z\in[0,\hat{z})\\ \hat{e}^{-1}l(z) & \text{if } z\in[\hat{z},z_0]\\ 0 & \text{if } z\in[z_{0,}\infty)\end{cases}.$$

The function $l(z)$ (4.17) is monotone decreasing on $[\hat{z},z_0]$, since $\Phi'(e)$ is a monotone decreasing function ($\Phi''(e)<0$) on $[0,\hat{e}]$.

The structure of the solution can be symbolically represented as $\hat{\mathbf{C}}^{\mathbf{A/M}}\vec{\mathbf{F}}\mathbf{C}_0^{\mathbf{A}}$, where $\mathbf{C}_0^{\mathbf{A}}=\mathbf{C}\{0,x=0\}$ is the initial constant state (the superscript indicates the material is in the austenitic phase), $\vec{\mathbf{F}}=\vec{\mathbf{F}}[\{0,0\}\uparrow\{\hat{e},\hat{x}\}]$ is the forward-propagating fan, and $\hat{\mathbf{C}}^{\mathbf{A/M}}=\mathbf{C}\{\hat{e},\hat{x}\}$ is the final constant state (the material is in an austenite/martensite mixture) and $\hat{x}=F^M(T_0,\hat{s})$. The trajectory $\mathsf{T}^s=\{(s(t),e(t)),\,t\in[0,\infty)\}$ of the solution lies on the A and A/M branches of the static stress-strain curve $s(e)$. Recall that the material on the gently sloping transformation branch of the isotherm $s(e)$ was previously identified as the A/M mixture. Since the stress profile in the centered fan, $\vec{\mathbf{F}}$ is spreading with time, so is the martensite fraction profile. Thus the A/M two-phase zone is becoming wider as it propagates along the rod.

If the shock loading amplitude $\hat{e}$ is such that $\bar{e}\le\hat{e}\le\tilde{e}$, then the initial stress-strain discontinuity $\vec{\mathbf{S}}_0$ formed due to the shock boundary condition (4.7) will split into a combination of a centered fan $\vec{\mathbf{F}}=\vec{\mathbf{F}}[\{0,0\}\,\mathbb{A}\,\{e^*,x^*\}]$[1] and a shock $\vec{\mathbf{S}}^*[\{e^*,x^*\}\,\mathbb{A}\,\{\hat{e},\hat{x}\}]$, where $x^*=F^M(T_0,s^*)$ and $\hat{x}=F^M(T_0,\hat{s})$ (see Figure 3). The shock $\vec{\mathbf{S}}^*$ represents the phase transformation front of a full or partial transformation, depending on values of x^* and $\hat{x}$. The solution has the structure $\hat{\mathbf{C}}\vec{\mathbf{S}}^*\mathbf{C}^*\vec{\mathbf{F}}\mathbf{C}_0^{\mathbf{A}}$, where $\hat{\mathbf{C}}=\hat{\mathbf{C}}^{\mathbf{M}}$ or $\hat{\mathbf{C}}^{\mathbf{A/M}}$ and $\mathbf{C}^*=\mathbf{C}^{\mathbf{A/M}}$. To fully define the solution, we need to find the point $e^*<\bar{e}$ where the fan $\vec{\mathbf{F}}$ and the phase front $\vec{\mathbf{S}}^*$ match; that is, to determine the velocity D^* (or z^*) of the front $\vec{\mathbf{S}}^*$.

---

[1] The centered fan (**F**-solution) can be continued beyond the point $\bar{e}$ where $\{F'(\bar{e})\}'=0$ (see (4.21)).

Uniqueness. Unfortunately, there is no unique solution to this problem. One of the possible solutions is the one depicted in Figure 4 when the velocity of the shock $\bar{\mathbf{S}}^*$ is sonic with respect to the material before the front, and therefore the constant state $\mathbf{C}^*$ is absent. This type of solution has the structure $\hat{\mathbf{C}}\bar{\mathbf{S}}^*\bar{\mathbf{F}}\mathbf{C}_o^{\mathbf{A}}$ and was first suggested by Bethe

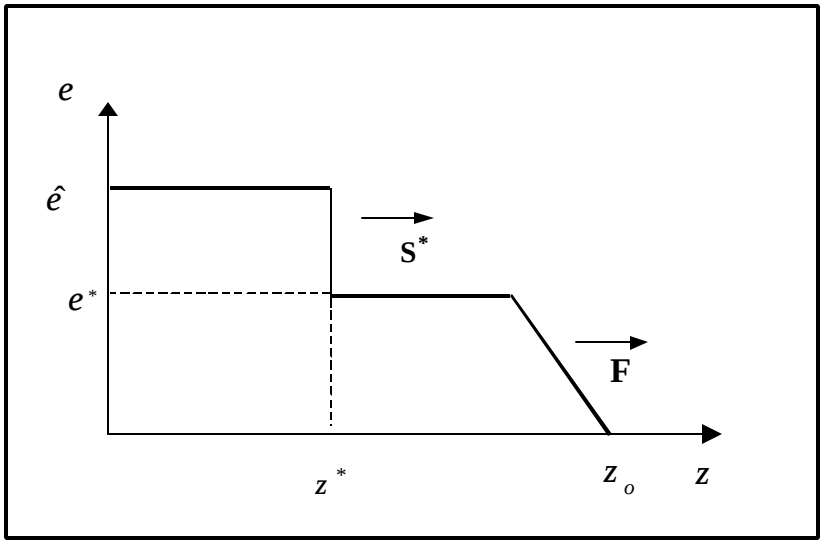

Figure 3. Strain profile for the $\hat{\mathbf{C}}\bar{\mathbf{S}}^*\mathbf{C}^*\bar{\mathbf{F}}\mathbf{C}_{\mathbf{o}}^{\mathbf{A}}$ solution

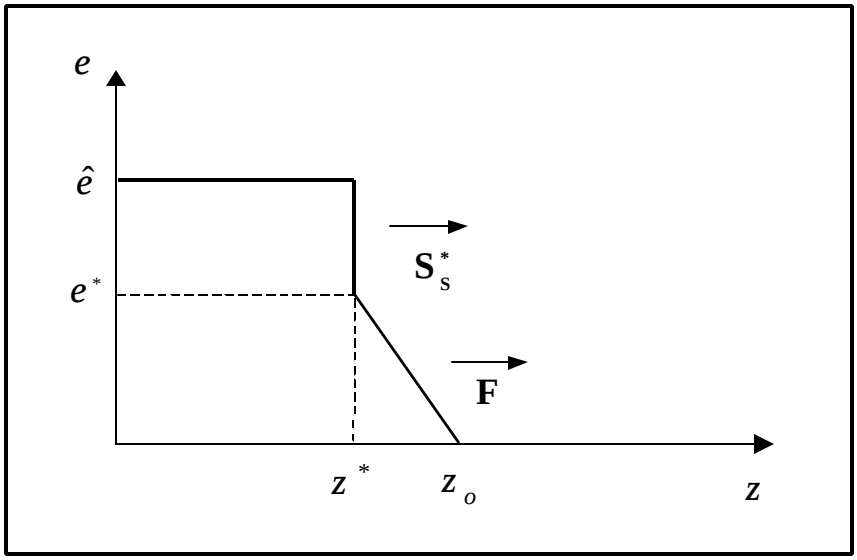

Figure 4. Strain profile for the $\hat{\mathbf{C}}\bar{\mathbf{S}}_S^*\bar{\mathbf{F}}\mathbf{C}_{\mathbf{o}}^{\mathbf{A}}$ solution

[34] in the gas dynamics framework. It was given explicitly by Barenblatt [32] for nonlinear elastic material (see also [35, 36]). We will refer to it as the Bethe-Barenblatt

solution and to the discontinuity $\vec{\mathbf{S}}^*$ as the sonic shock (or phase front) $\vec{\mathbf{S}}^*_{\mathrm{S}}$. The velocity D^* of the sonic shock coincides with the acoustic velocity

$$c^* = \sqrt{f'(e^*)/r}$$

on the tail (last) characteristic of the centered fan $\vec{\mathbf{F}}$. In other words, the trajectory of a sonic shock $\vec{\mathbf{S}}^*_{\mathrm{S}}$ in the x-t plane coincides with the tail characteristic $\mathbf{C}^+$ of the fan $\vec{\mathbf{F}}$. According to Equation (4.13),

$$D^* = \sqrt{\frac{f(\hat{e}) - f(e^*)}{r(\hat{e} - e^*)}},$$

and hence e^* is defined implicitly by the equation

$$\Phi'(e^*) = \frac{\Phi(\hat{e}) - \Phi(e^*)}{\hat{e} - e^*}, \tag{4.18}$$

which allows a matching point z^* to be found from Equation (4.16):

$$z^* = \sqrt{\Phi'(e^*)}. \tag{4.19}$$

There is a simple geometric interpretation of Equation (4.18): the velocity of a sonic shock (phase front) $\vec{\mathbf{S}}^*_{\mathrm{s}}$ is given by a tangent line construction (see Figure 5), namely, the $\vec{\mathbf{S}}^*_{\mathrm{s}}$-Rayleigh chord

$$R(e) = D^*(e - \hat{e}) + \hat{f}, \quad \hat{f} = f(\hat{e}),$$

where the final point $(\hat{e}, \hat{f})$ is tangent to the curve $f(e)$ at the point (e^*, f^*). The equation for the Rayleigh chord can then be written as

$$R(e) = f'(e^*)(e - \hat{e}) + \hat{f}.$$

We will henceforth refer to the sonic discontinuity $\vec{\mathbf{S}}^*_{\mathrm{S}}$ as the tangent shock $\vec{\mathbf{S}}^{\mathbf{t}}$. The sonic phase front $\vec{\mathbf{S}}^*_{\mathrm{S}}$ in the Bethe-Barenblatt solution $\hat{\mathbf{C}}\vec{\mathbf{S}}^*_{\mathrm{S}}\vec{\mathbf{F}}\mathbf{C}_0$ satisfies the generalized Lax stability condition [37, 12]

$$c(e_-) \geq D \geq c(e_+),$$

since, at the endpoints of the $\vec{\mathbf{S}}^*_{\mathrm{S}}$-Raleigh chord,

$$c(\hat{e}) > D^* = c(e^*), \quad e_- = \hat{e}, e_+ = e^*.$$

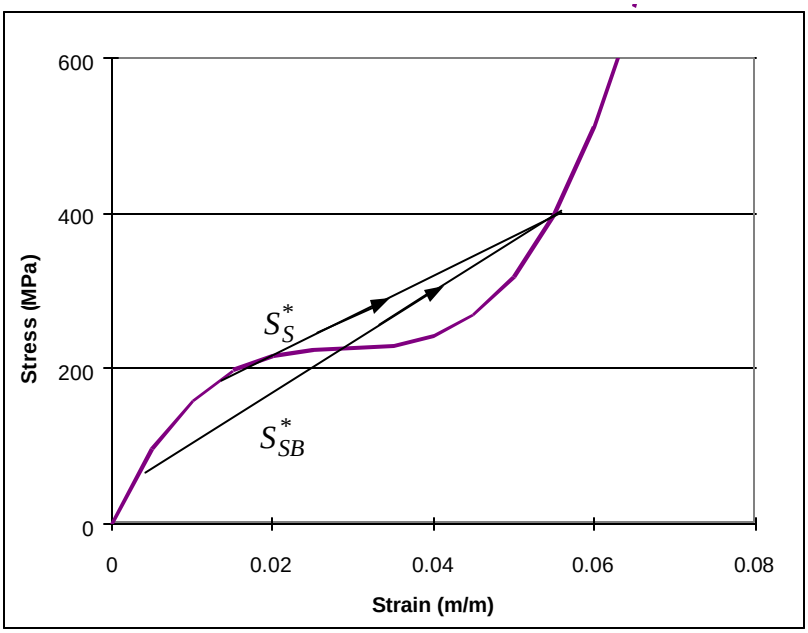

Figure 5. Isotherm for an SMA with a cubic constitutive relation and Rayleigh lines for sonic and subsonic shocks.

It is important to note that a similar solution with a supersonic phase front $\vec{\mathbf{S}}_{\mathrm{SP}}$ with $D > c(e_+)$ (see Figure 5) is impossible. Heuristically, this can be explained in the following way: a phase front $\vec{\mathbf{S}}_{\mathrm{SP}}$ with a supersonic velocity will be overtaking the tail of the fan $\vec{\mathbf{F}}$ until it reaches the characteristic that has slope $c(e)$, where $D = c(e)$.

From now on, to simplify the discussion, we disregard change in cross-sectional area of the rod, so that $f(e) \equiv s(e)$ and $D \equiv D_C$. Then the condition given by (4.18) takes the form

$$s'(e^*) = \frac{s(\hat{e}) - s(e^*)}{\hat{e} - e^*}. \tag{4.20}$$

For example, for the cubic stress-strain law of the form $s(e) = ge^3 - be^2 + ae$ the matching point $z^* = D^*/V$ can be found from (4.19) and (4.20) to be

$$z^{*2} = \frac{1}{12h}\left[(3h\hat{e} - m)^2 + 4(3h - m^2)\right].$$

The velocity scale V has been chosen here so that

$$V^2 = a/r,$$

so that

$$\Phi(e) = e - me^2 + he^3,$$
$$m = b/rV^2,\ h = g/rV^2$$

and
$$l(z) = \frac{m}{3h}\left(\sqrt{1 + 3h(z^2 - 1)/m} - 1\right).$$

It was shown in [39] that for an isothermal case, the second law of thermodynamics is equivalent to the following condition on any forward-moving ($D \geq 0$) stress-strain discontinuity $\vec{\mathbf{S}}[e_+ \uparrow e_-]$:

$$P(e_+, e_-) = \int_{e_+}^{e_-} s(e)de + \frac{s(e_+) + s(e_-)}{2}(e_- - e_+) \geq 0,$$

where $R = R(e_+, e_-)$ is the thermodynamic driving force for the transformation and

$$PD = \left(\int_{S_+}^{S_-} TdS\right)D = T\Delta SD \geq 0$$

is the dissipation rate. It is easy to see that $R(e_+, e_-)$ represents the difference between the area under stress-strain isotherm $s(e)$ and the $\vec{\mathbf{S}}$-Raleigh chord $R(e)$ on the interval $[e_-, e_+]$. It follows immediately from Figure 5 that a sonic phase front $\vec{\mathbf{S}}_{\mathrm{S}}^*$ dissipates mechanical energy and hence is thermodynamically admissible.

In the above-discussed Bethe-Barenblatt solution $\hat{\mathbf{C}}^{\mathbf{M}}\vec{\mathbf{S}}_{\mathrm{S}}^*\vec{\mathbf{F}}\mathbf{C}_{\mathbf{0}}^{\mathbf{A}}$, the velocity of the sonic interface $\vec{\mathbf{S}}_{\mathrm{S}}^*$ is uniquely defined by the geometry of the isotherm $e = I(T_0, s)$; that is, by the constitutive and kinetic laws given by (4.1). This is not the case for other thermodynamically admissible solutions $\hat{\mathbf{C}}^{\mathbf{M}}\vec{\mathbf{S}}_{\mathrm{SB}}^*\mathbf{C}^*\vec{\mathbf{F}}\mathbf{C}_{\mathbf{0}}^{\mathbf{A}}$ with subsonic moving phase fronts $\vec{\mathbf{S}}_{\mathrm{SB}}^*$ (see Figures 3 and 5). For the subsonic interfaces, the additional kinetic relation is required to single out a unique solution (the velocity of the interface $\vec{\mathbf{S}}_{\mathrm{SB}}^*$). The kinetic relation expresses the velocity D of a subsonic interface as a function of the thermodynamic driving force [39, 40]:

$$D = \Psi(P(e_+, e_-)). \tag{4.21}$$

In our case,

$$D^* = \Psi(P(e^*, \hat{e})), \tag{4.22}$$

where

$$D^*(e^*,\hat{e}) = \sqrt{\frac{s(\hat{e}) - s(e^*)}{\hat{e} - e^*}}. \tag{4.23}$$

Equation (4.22) replaces Equation (4.20) and, for a given amplitude of shock loading $\hat{e}$ (i.e., strain behind the interface), allows us to uniquely determine a strain e^* in front of the interface if the kinetic function $\Psi(\bullet)$ is monotone.

As emphasized in [40], on a phenomenological level, the kinetic relation should be considered as an additional constitutive assumption for the SMA material that, in principle, can be obtained experimentally. On the other hand, it is shown that, using a viscosity-capillarity augmentation of the hyperbolic system given by (4.5), one can derive the kinetic relation (4.21) from the analysis of the internal structure of a subsonic discontinuity (solvability condition). For a thorough discussion of this subject, we refer to recent works [13, 41].

If one accepts the generalized Lax condition, the viscosity/Oleinik chord criteria or the Dafermos maximum dissipation criteria, then the Bethe-Barenblatt solution with the sonic shock (phase front) is unique [42, 13][1]. However, one can argue that, for phase transition fronts, the criteria listed above are too restrictive. Therefore, the subsonic interfaces are widely accepted and studied in the phase transformation literature [39, 43, 41]. Sometimes subsonic phase fronts are called *kinks* to distinguish them from the conventional shocks that satisfy the Lax criteria.

We also note here that, in a recent work by Chen and Lagoudas [44], the use of jump conditions in conjunction with the second law of thermodynamics rendered unique subsonic solutions for a similar problem of impact loading on an SMA rod. However, we would like to suggest here that perhaps both the sonic and subsonic front solutions are physically meaningful, and represent two different regimes of transformation propagation (as suggested by [12] in a slightly different framework).

[1] for strictly convex-concave $f(e)$ (i.e., for the conventional shocks) all these criteria are equivalent.

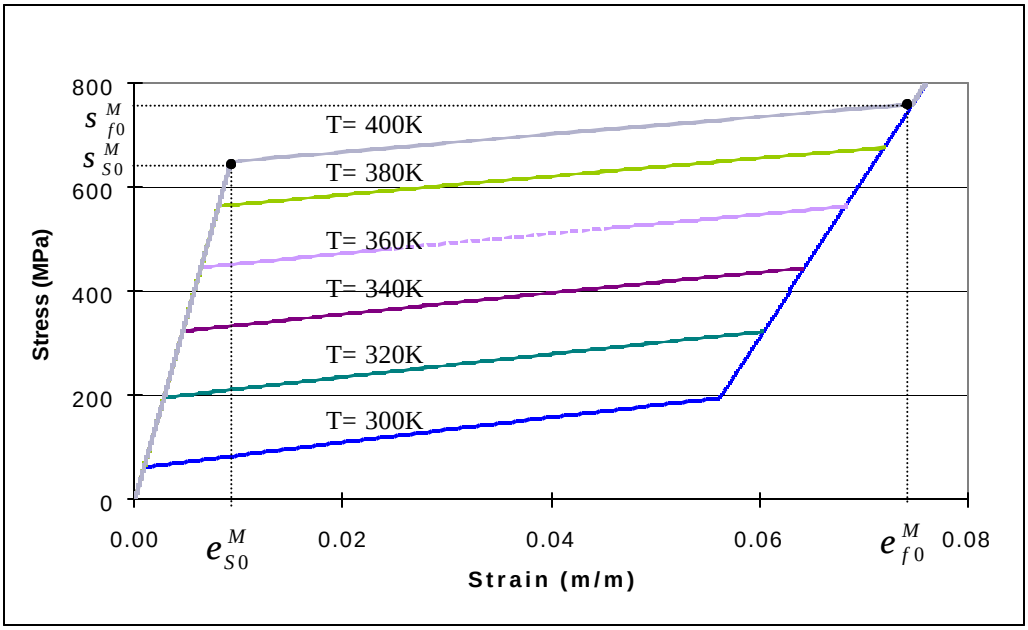

Figure 6. Stress-strain curves for linear SMA kinetics. The critical points are marked for the T=400K isotherm.

4.2.2 Isotherms with kinks. Most SMA materials exhibit nearly elastic behavior in the purely austenite and martensite phases. For such materials, usually modeled by linear, exponential or cosine kinetics, the start of the phase transformation at the point (e^M_{S0}, s^M_{S0}) on the isotherm and the finishing point (e^M_{f0}, s^M_{f0}) (see (2.3)) are points of discontinuity of (4.3). Here we used the notation $s^M_{S0} = s^M_S(T_0)$, $s^M_{f0} = s^M_f(T_0)$ and by virtue of (4.1) we have $e^M_{S0} = Ks^M_{S0}$, $e^M_{f0} = \mathrm{K}s^M_{f0} + \Lambda$. Figure 6 shows a sample of several linear isotherms at different temperatures. The critical points are shown for the $T = 400K$ isotherm.

As the critical stress level s^M_{S0} is reached, the stress-strain isotherms $e = I(T_0, s)$ have a convex portion P at least in a small vicinity of the critical point (e^M_{S0}, s^M_{S0}). In this case, the front part of the centered fan $\vec{\mathbf{F}} = \vec{\mathbf{F}}[0 \uparrow e^*]$ degenerates into a linear elastic shock $\vec{\mathbf{S}}^{\mathbf{EL}} = \mathbf{S}[0 \uparrow e^*]$ (elastic precursor). The solution thus has the two-shock structure:

$$\hat{\mathbf{C}}^{\mathbf{M}}\bar{\mathbf{S}}^{*}_{\mathrm{SB}}\,\mathbf{C}^{*\mathbf{A}}\bar{\mathbf{S}}^{\mathbf{EL}}\,\mathbf{C}^{\mathbf{A}}_{0}.$$

In other words, the initial shock $\vec{\mathbf{S}}_{\mathbf{o}}[0\,\hat{e}]$ for a large enough amplitude of loading splits in two: the linear elastic precursor $\vec{\mathbf{S}}^{\mathbf{EL}}[0\uparrow e^{*}]$ and the subsonic shock/phase front $\vec{\mathbf{S}}^{*}_{\mathrm{SB}} = \vec{\mathbf{S}}[e^{*}\,\hat{e}]$. In this case, two types of solutions are possible:

Lee-Tupper solution: $e^{*} = e^{M}_{S0},\ s^{*} = s^{M}_{S0}$

The Rayleigh line for a front $\vec{\mathbf{S}}^{*}_{\mathrm{SB}}$ starts at the corner (critical) point (e^{M}_{S0}, s^{M}_{S0}) of the isotherm $e = I(T_0, s)$. Hence, the velocity of the isothermal phase transformation front is given by

$$D^{\mathrm{PT}}\Big|_{T=T_0} = \sqrt{\frac{\hat{s} - s^{M}_{S0}}{r\,(\hat{e} - e^{M}_{S0})}}. \tag{4.24}$$

Note that $D^{\mathrm{PT}}(e^{M}_{S0}, \hat{e}) < c(e^{M}_{S0} - 0) = \dfrac{1}{\sqrt{r\mathrm{K}}}$.

We will call such a front (shock) the corner front (shock) $\vec{\mathbf{S}}^{\mathbf{c}}$. The constant state $\mathbf{C}^{*} = \mathbf{C}\{e^{M}_{S0}, s^{M}_{S0}, x = 0\}$ will be called the critical state $\mathbf{C}^{\mathbf{c}}$. This two-shock configuration of the solution for materials with nonconvex stress-strain curves with a corner (kink) point was first discussed by Lee and Tupper [46] in the framework of plastic wave propagation. Therefore, we refer to this configuration as the Lee-Tupper solution. Almost at the same time, Bancroft et al [47] considered the two-shock configuration that resulted from the splitting of strong shock waves in iron. The splitting is caused by a kink point on the Hugoniot curve, which is due to shock-induced phase transition in iron.

Obviously, a corner shock $\vec{\mathbf{S}}^{\mathbf{c}}$ can be considered as a limiting case for a tangent shock $\vec{\mathbf{S}}^{\mathbf{t}}$. In this connection, we note that the Lee-Tupper solution can be considered a good approximation to the Bethe-Barenblatt solution for an SMA with cosine kinetics (2.9) if the transformation strip is sufficiently wide. Note that the velocity of a corner

shock (as the velocity of a tangent shock) is fully defined by the geometry of the curve $s(e)$, and no additional kinetic relation is needed.

Abeyaratne-Knowles type solution: $e^* < e_{S0}^M, s^* < s_{S0}^M$

In this case, the $\vec{\mathbf{S}}_{\mathrm{SB}}^*$-Rayleigh line starts at some point (e^*, s^*) on the A-branch of the isotherm below the critical point (e_{S0}^M, s_{S0}^M). The point e^* can be determined from the system of equations (4.22, 4.23), and the velocity of phase front is given by (4.22). Note that Abeyaratne-Knowles type solutions deviate from Lee-Tupper type solutions only for large enough amplitudes of loading $\hat{e} > e_{f0}^M$.

Since the linear kinetics model is widely used, we will provide some details of the Lee-Tupper type solution for SMA with a trilinear isotherm $s = I_L^{-1}(T_0, e)$ given by:

$$I_L^{-1}(T_0, e) = \begin{cases} e\mathrm{K}^{-1} & \text{if } e < e_{S0}^M \\ (e + k s_{S0}^M)(\mathrm{K} + k)^{-1} & \text{if } e_{S0}^M < e < e_{f0}^M \\ (e + \Lambda)\mathrm{K}^{-1} & \text{if } e > e_{f0}^M \end{cases} \tag{4.25}$$

Depending in the amplitude of the impact load we have three cases:

1. If $\hat{e} < e_{S0}^M$, then the solution has the structure

$$\hat{\mathbf{C}}^{\mathbf{A}} \vec{\mathbf{S}}^{\mathbf{EL}} \mathbf{C}_{\mathbf{o}}^{\mathbf{A}},$$

where $\vec{\mathbf{S}}^{\mathbf{EL}} = \vec{\mathbf{S}}[0 \nearrow \hat{e}]$ is a linear elastic shock with velocity

$$D^{\mathrm{EL}} = \frac{1}{\sqrt{r\mathrm{K}}}.$$

For NiTi SMA material (see data in Table 1), the velocity of the elastic precursor $D^{\mathrm{EL}} = 3.3 \cdot 10^3 \,\mathrm{m/s}$.

2. If $\hat{e} > e_{f0}^M$, then the solution has the structure

$$\hat{\mathbf{C}}^{\mathbf{M}} \vec{\mathbf{S}}^{\mathbf{c}} \mathbf{C}^{\mathbf{c}} \vec{\mathbf{S}}^{\mathbf{EL}} \mathbf{C}_{\mathbf{o}}^{\mathbf{A}},$$

where

$$\vec{\mathbf{S}}^{\mathbf{EL}} = \vec{\mathbf{S}}[0 \uparrow e_{S0}^M]$$
$$\vec{\mathbf{S}}^{\mathbf{c}} = \vec{\mathbf{S}}[\{e_{S0}^M, x = 0\} \uparrow \{\hat{e}, 1\}],$$

and where the velocity of the phase transformation front $\vec{\mathbf{S}}^{\mathbf{c}}$ given by (4.24) can be rewritten as

$$D_2^{\mathrm{PT}}\Big|_{T=T_0} = \frac{1}{\sqrt{r\left(\mathrm{K} + c(\hat{s})\right)}}, \quad c(\hat{s}) = \Lambda/(\hat{s} - s_{S0}^{M}). \tag{4.26}$$

Note that the velocity D_2^{PT} essentially depends on the loading amplitude $\hat{s}$. The $\vec{\mathbf{S}}^{\mathbf{c}}$-Rayleigh line starts at the corner point (e_{S0}^{M}, s_{S0}^{M}) of the isotherm $e = I_L(T_0, s)$ and ends at the point $(\hat{e}, \hat{s})$ of the M-branch of the isotherm. Material behind the phase front is fully transformed to martensite.

3. If $e_{S0}^{M} < \hat{e} < e_{f0}^{M}$, then the solution has the structure

$$\hat{\mathbf{C}}^{\mathbf{A/M}}\vec{\mathbf{S}}^{\mathbf{c}}\mathbf{C}^{\mathbf{c}}\vec{\mathbf{S}}^{\mathbf{EL}}\mathbf{C}_{\mathbf{0}}^{\mathbf{A}}$$

$$\vec{\mathbf{S}}^{\mathbf{c}} = \vec{\mathbf{S}}[\{e_{S0}^{M}, 0\} \uparrow \{\hat{e}, \hat{x}\}],$$

where $\hat{x} = Z^{M}(T_0, \hat{s})$. The velocity of the phase transformation front $\vec{\mathbf{S}}^{\mathbf{c}}$ is given by

$$D_3^{\mathrm{PT}}\Big|_{T=T_0} = \frac{1}{\sqrt{r\,(\mathrm{K} + k)}}, \quad k = \Lambda b^{M}, \tag{4.27}$$

and is independent of the loading amplitude. In other words, $\vec{\mathbf{S}}^{\mathbf{c}}$ is a linear shock; the $\vec{\mathbf{S}}^{\mathbf{c}}$-Rayleigh line starts at the corner point (e_{S0}^{M}, s_{S0}^{M}) of the isotherm $e = I(T_0, s)$ and lies on the linear A/M-transformation branch of the isotherm. Material behind the front is partially martensite (two-phase A/M mixture). For NiTi SMA material (see Table 1), the velocity of the phase transformation front $D_3^{\mathrm{PT}}\Big|_{T=T_0} = 0.65 \cdot 10^3\,\mathrm{m/s}$. Note that, for the trilinear constitutive law, the locus points on the (e, s) plane that can be reached by the shock loading of an unstressed 1-D SMA body with initial temperature T_0 (shock-isotherm) coincide with the static isotherm $e = I_L(T_0, s)$.

Thorough discussion of a solution of the impact loading problem with a subsonic shock (kink) $\vec{\mathbf{S}}_{\mathrm{SB}}^{*} = \vec{\mathbf{S}}[\{e^{*}, 0\} \uparrow \{\hat{e}, 1\}]$ with $e^{*} < e_{S0}^{M}$ can be found in [11]. Even though the authors consider a trilinear material with transformation softening behavior (*N*-shaped constitutive relation), their solution is fully applicable to our case (trilinear material with

transformation hardening behavior) for $\hat{e} > e_{\mathrm{f0}}^{M}$, since the intermediate phase (falling branch of the isotherm) does not appear in the solution.

Note that the expression (4.31) gives the lower limit for the velocity of an isothermal phase front of partial transformation for both Lee-Tupper and Abeyaratne-Knowles solutions.

Finally, we mention that the splitting instability of strong shock waves associated with first-order phase transformation in gases (vapors) and solids has been studied extensively in a hydrodynamic framework [18, 48, 49, 19]. In both cases, only the tangent and corner shocks have been considered. Since these phase transitions can be induced generally only by strong shock waves, an adiabatic approximation has been employed, but not an isentropic one.

4.3 Numerical results. As a conclusion to this section we give two numerical experiments of the above theoretical results. For both cases we used a standard Lax-Friedrichs finite difference scheme [45] applied to the finite difference version of equation (4.5). The domain is the rectangle $(x,t) \in [0,L] \times [0,T]$, L being the length of the rod and $[0,T]$ the time interval for which we want a solution. The solution is obtained on a uniform grid with points (x_i, t_j), where $x_i = ih$ and $t_j = jt$ for $i = 0,1,...,{}^{L}\!/_{h}$ and $j = 0,1,...,{}^{T}\!/_{t}$. The primitive variables are the strain $e(x,t)$ and velocity $\mathrm{v}(x,t)$ and we approximate all spatial derivatives by the central finite difference - $f_x(x_i,t_j) = \dfrac{f(x_{i+1},t_j) - f(x_{i-1},t_j)}{2h} + O(h^2)$ and all time derivatives by $f_t(x_i,t_j) = \dfrac{f(x_i,t_{j+1}) - \frac{1}{2}\left(f(x_{i+1},t_j) + f(x_{i-1},t_j)\right)}{t} + O(t)$, where $f = \mathrm{v}, e$, at the nodes (x_i,t_j). At the end of each time step when the values for the strain and velocity are already computed we update the stress using the return mapping algorithm presented in [52]. The material properties used are given in the next table.

Table 1. Material data for NiTi Shape Memory Alloy used in calculations.

$E=E^A=E^M$	70.0E9 Pa	T_0	42 °C
Λ	0.05 m/m	T_{S0}^M	18 °C
k^M	5.25E6 Pa	T_{F0}^M	-2 °C
a	10.0E-6 1/°C	r	6450.0 kg/m^3
rDS_R	0.35E6 Pa/°C	C	328.68 J/kg°C

We solved the impact problem (4.5,6,7) first with a cubic isotherm (see Figure 5). Results are depicted in Figure 7. As one might expect, due to the large numerical viscosity introduced by the scheme, the finite difference approximation picked up the Bethe-Barenblatt solution with the sonic shock (phase front).

The second problem we solved was for an SMA material with a linear transformation behavior (see Figure 6). It is easy to see that the finite difference solution is the Lee-Tupper solution with a corner shock (front) $\vec{\mathbf{S}}^{\mathbf{c}}$. The strain profile of the numerical solution is shown on Figure 8. The numerical velocity of the phase front $\vec{\mathbf{S}}^{\mathbf{c}}$ coincides with the velocity given by the analytical expression (4.27) within 1%, Thus the numerical solution is in perfect agreement with the analytical results developed previously.

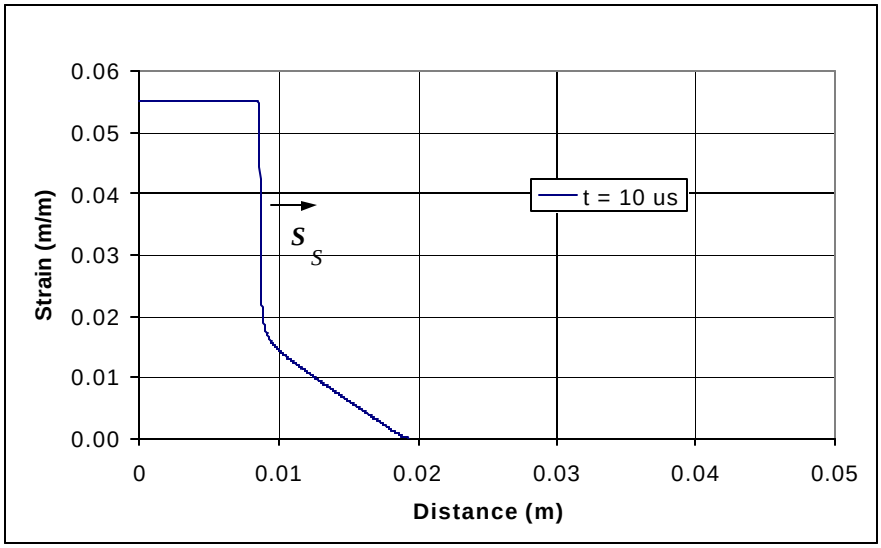

Figure 7. Numerical strain profile for the impact loading of an SMA with a cubic constitutive relation, $\hat{s} = 400$ MPa (Lax-Friedrichs scheme)

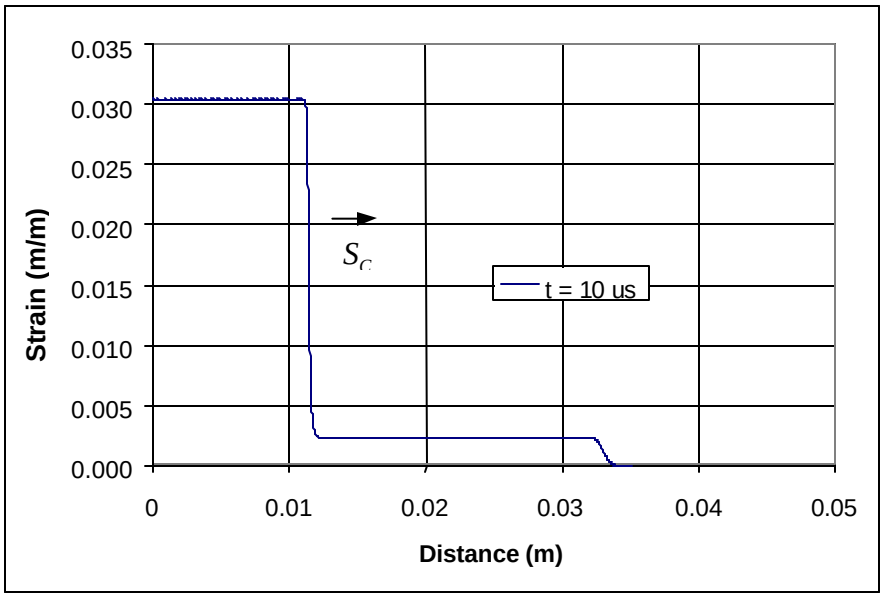

Figure 8. Numerical strain profile for the impact loading of an SMA with a trilinear constitutive relation, $\hat{s} = 400$ MPa (Lax-Friedrichs scheme)

5. ADIABATIC CASE

5.1 Analytical Results. To simplify the study in this section we disregard the change in cross-sectional area of the rod during the impact loading. Then the system of equations (3.3,8) for the adiabatic case takes the form

$$\begin{aligned} r\,u_{tt} &= s_x \\ S_t &= 0 \end{aligned} \tag{5.1}$$

The initial and boundary conditions for the impact problem are

$$\begin{aligned} \textbf{IC:}\quad & e(x,0) = \mathrm{v}(x,0) = 0,\ x \ge 0 \\ & T(x,0) = T_0,\ x \ge 0 \\ \textbf{BC:}\quad & s\,(0,t) = \hat{s}\,H(t),\ t \ge 0;\ (\hat{s} > 0). \end{aligned} \tag{5.2}$$

The entropy given by (3.8) stays constant (5.1) along the rod during the impact process:

$$S(x,t) = S(x,0) \equiv \mathrm{S}_0, \quad x,t \ge 0, \tag{5.3}$$

where $\mathrm{S}_0 = C \ln\left(T_0/T_R\right) + S_R^A$.

In this section, we will use the combined constitutive and kinetic laws in the form

$$e = E(T_0; T, s) := \mathrm{K}s + a(T - T_0) + \Lambda\Xi(T, s).$$

Note that

$$E(T_0; T, s) = \boldsymbol{I}(T, s) + a(T - T_0) \text{ and}$$
$$E(T_0; T_0, s) = \boldsymbol{I}(T_0, s).$$

In order to simplify the equations and obtain analytical results, we limit our consideration to a linear kinetic law only (see 2.4,7). Since $Z^M(T,s)$ is a monotone increasing function of s in **[M],** we can write Equation (5.3) as

$$S = a\,s/r + C\ln\{T/T_R\} - DS_R X_L(T, s) + S_R^A = S_0 \tag{5.4}$$

and invert it to find $T = T_L(S_0, s)$. Then the strain is given by

$$e = E_L(S_0, s) := E(T_R e^{\frac{S_0 - S_R^A}{C}}; T_L(S_0, s), s). \tag{5.5}$$

The function $e = E_L(S_0, s)$ can be inverted to find the isentrope $s = E_L^{-1}(S_0, e)$, which has a form very similar to that of the trilinear isotherm (4.25). It is easy to see that the isentrope has an A-branch that is almost identical to that of the isotherm and that the isentrope has a kink at the starting point of transformation, just as the isotherm does (see Figure 9 and 10). We will return to the discussion of the isentrope later.

The isentropic system of equations (5.1) is equivalent to

$$r\,u_{tt} = s'u_{xx}, \tag{5.6}$$

where $s' = \partial_e s(S_0, e)$. For the linear kinetic law considered here, we have that $s' = \partial_e E_L^{-1}(S_0, e)$, which can easily be found in an explicit form by differentiating Equations (5.4 and 5.5) to obtain

$$s' = \partial_e E_L^{-1} = \begin{cases} \mathrm{K}^{-1} & \text{if } e < e_{\mathrm{S0}}^M \\ \left(\mathrm{K} + n(S_0, e)\right)^{-1} & \text{if } e_{\mathrm{S0}}^M < e < e_{\mathrm{m0}}^M \\ \mathrm{K}^{-1} & \text{if } e > e_{\mathrm{m0}}^M \end{cases} \tag{5.7}$$

where

$$e_{\mathrm{m0}}^M = E_L(S_0, s_{\mathrm{mf\,0}}^M) \text{ and } s_{\mathrm{mf\,0}}^M = s_f^M(T_{m0}^M). \tag{5.8}$$

The quantity T_{m0}^{M} is the maximum achievable M-transformation temperature (3.14). In Equation (5.7), we disregarded the very small thermoelastic terms in the pure A and M phases. Note that we do not need here the concrete form of the function $n = n(S_0, e)$; what is important is that this function is positive, monotone increasing and almost constant ($n \cong n_0 > 0$), so that Equation (5.6) is hyperbolic and $s'' = \partial_e^2 E_L^{-1} > 0$ for $e \in [e_{\mathrm{S0}}^{M}, e_{\mathrm{m0}}^{M}]$. Therefore, the results obtained in the previous section can be directly applied here. Particularly, the solution of the shock-impact problem (5.3) is piece-wise constant and has a two-shock structure $\hat{\mathbf{C}}\bar{\mathbf{S}}^{*}\mathbf{C}^{*}\bar{\mathbf{S}}^{\mathbf{EL}}\mathbf{C}_0$, with the elastic precursor $\bar{\mathbf{S}}^{\mathbf{EL}} = \bar{\mathbf{S}}[0 \mathbb{A} e^{*}]$ and the subsonic shock (phase front) $\bar{\mathbf{S}}^{*} = \bar{\mathbf{S}}[\{e^{*}, x^{*} = 0, T_0\} \mathbb{A} \{\hat{e}, \hat{x}, \hat{T}\}]$. Hence, we need to consider only the Rankine-Hugoniot jump conditions (4.12) at the phase transition front $\bar{\mathbf{S}}^{*}$ along with a continuity condition for the entropy:

$$\hat{S} - S^{*} = 0. \tag{5.9}$$

We obtain results similar to (4.13,23):

$$D^{\mathrm{PT}} = \sqrt{\frac{\hat{s} - s^{*}}{r(\hat{e} - e^{*})}} \tag{5.10}$$

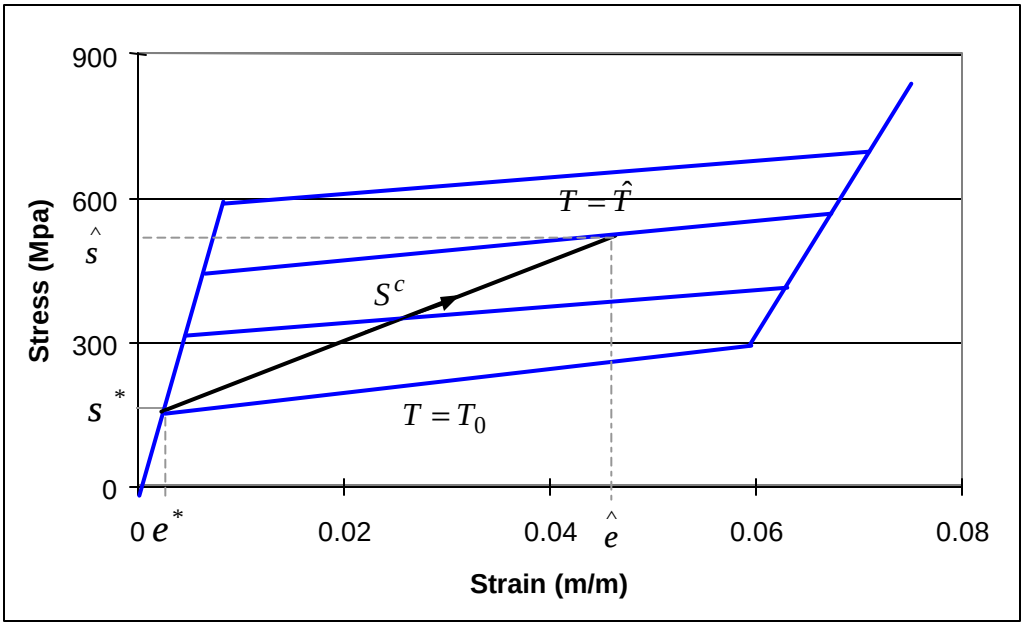

Figure 9. Rayleigh line for the isentropic partial transformation front $\bar{\mathbf{S}}^{\mathbf{c}}$

$$\hat{\mathrm{v}} = \mathrm{v}^* - D^{\mathrm{PT}}\left(\hat{e} - e^*\right) \text{ and} \tag{5.11}$$

$$\frac{a}{r}(\hat{s} - s^*) + C\ln\left(\hat{T}/T_0\right) - \Delta S_R \hat{x} = 0. \tag{5.12}$$

From the condition of constancy of entropy across the phase front in (5.12), we find that

$$\begin{aligned} &\hat{T} = T_0 \exp(w\hat{x} - q(\hat{s} - s^*)) \\ &w = a/r\Delta S_R,\ q = a/r\Delta S_R, \end{aligned} \tag{5.13}$$

which means that the temperature in the phase front changes (reversibly) only due to the latent heat release and the thermoelastic heat generation. As before, we will disregard the very small change in temperature caused by thermoelastic heat generation, but we will take into account the thermoelastic strain due to the significant increase in temperature produced by the latent heat release. If we omit in (5.13) the small thermoelastic term $q(\hat{s} - s^*)$, we recover expression (3.13)

$$\hat{T} = T_0 \exp(w\hat{x}) \text{ or } \hat{x} = w^{-1}\ln(\hat{T}/T_0),$$

and the maximum attainable temperature behind the front is given by $\hat{T}\big|_{\hat{x}=1} = T_0 \exp(w) \equiv T_{\mathrm{m}0}^M$ (see (3.14)). Then, obviously, we have $\hat{T} \in [T_0, T_{\mathrm{m}0}^M]$. For convenience, we will introduce here the corresponding maximum achievable M-transformation stress

$$s_{\mathrm{m}0}^M = s_{\mathrm{m}f0}^M + \Theta(T_{m0}^M - T_0) + \Omega$$

and the maximum achievable M-transformation strain (cf. (5.8))

$$e_{m0}^M = E(T_0; T_{m0}^M, s_{\mathrm{m}f0}^M)).$$

As in the previous section, we will discuss here only the Lee-Tupper type solution $\hat{\mathbf{C}}\bar{\mathbf{S}}^*\mathbf{C}^*\bar{\mathbf{S}}^{\mathbf{EL}}\mathbf{C}_0^{\mathbf{A}}$ with a corner shock (front) $\bar{\mathbf{S}}^{\mathbf{c}} = \bar{\mathbf{S}}^*$ with $e^* = e_{S0}^M$ and $s^* = s_{S0}^M$. For the Abeyaratne-Knowles solution having the subsonic interface $\bar{\mathbf{S}}_{\mathrm{SB}}^*$ with $e^* < e_{S0}^M$, we refer again to [11]. In the following lines, we will provide the details of the Lee-Tupper type solution.

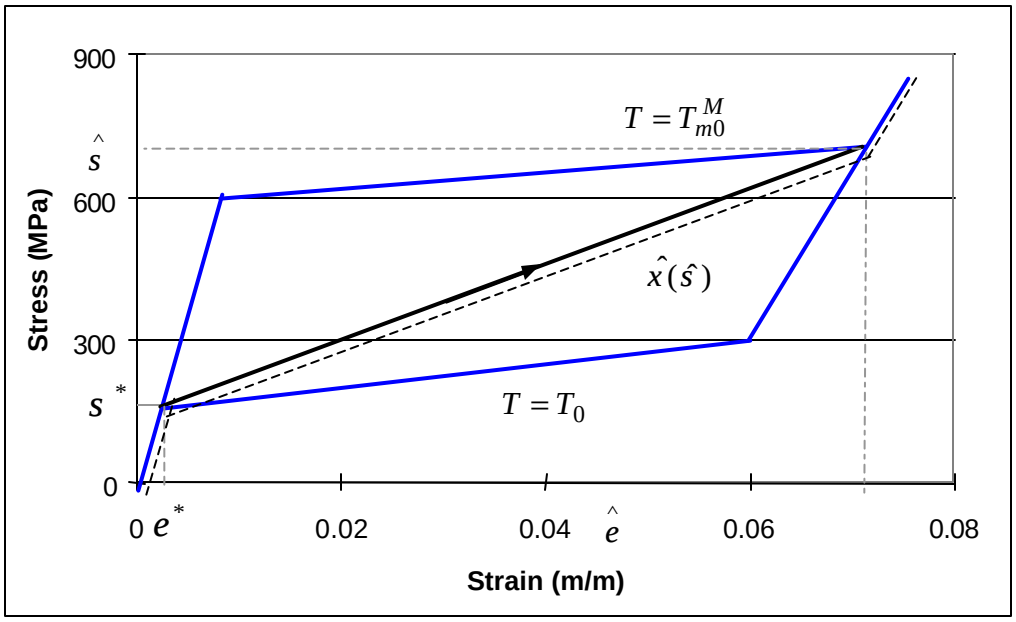

Figure 10. Shock adiabat-isentrope $\hat{e} = S_L(T_0, \hat{s}) \cong E_L(S_0, \hat{s})$ for the Lee-Tupper type solution (dashed line) and Rayleigh line for the isentropic front $\vec{\mathbf{S}}^{\mathbf{c}}$ of full transformation

1. If $\hat{s} < s_{S0}^M$, then $\hat{x} = 0$ and $\hat{T} = T_0$ (austenite material behind the linear elastic shock); the solution is isothermal and has the structure $\hat{\mathbf{C}}^{\mathbf{A}}\vec{\mathbf{S}}^{\mathbf{EL}}\mathbf{C}_0^{\mathbf{A}}$, where

$$\vec{\mathbf{S}}^{\mathbf{EL}} = \vec{\mathbf{S}}[\{0,0,T_0\} \uparrow \{\hat{e},0,T_0\}] \text{ with } \hat{e} = K\hat{s}.$$

2. If $\hat{s} > s_{m0}^M$ then $\hat{x} = 1$, $\hat{T} = T_{m0}^M$ and $\hat{e} = E(T_0; \hat{T}, \hat{s})$ (fully heated martensite material behind the phase front). The solution has the Lee-Tupper structure $\hat{\mathbf{C}}^{\mathbf{M}}\vec{\mathbf{S}}^{\mathbf{c}}\mathbf{C}^{\mathbf{c}}\vec{\mathbf{S}}^{\mathbf{EL}}\mathbf{C}_0^{\mathbf{A}}$, where

$$\vec{\mathbf{S}}^{\mathbf{EL}} = \vec{\mathbf{S}}[\{0,0,T_0\} \text{ A } \{e_{S0}^M,0,T_0\}]$$
$$\vec{\mathbf{S}}^{\mathbf{c}} = \vec{\mathbf{S}}[\{e_{S0}^M,0,T_0\} \text{ A } \{\hat{e},1,\hat{T}\}]$$

The $\vec{\mathbf{S}}^{\mathbf{c}}$-Rayleigh line starts at the corner point (e_{S0}^M, s_{S0}^M) of the initial cold isotherm $e = I_L(T_0, s)$ and ends at the point $(\hat{e}, \hat{s})$ of the M-branch of the hot isotherm $e = I_L(T_{m0}^M, s)$ (see Figure 10). Note that the A-branches of both isotherms overlap, and their M-branches are also almost indistinguishable, since the thermoelastic strain caused by latent heat release is quite small.

3. If $s^{M}_{S0} < \hat{s} < s^{M}_{m0}$, then $0 < \hat{x} < 1$, $T_0 < \hat{T} < T^{M}_{m0}$, $\hat{e} = E(T_0, \hat{T}, \hat{s})$ and $\hat{T} = T_0 \exp(w\hat{x})$ (heated two-phase mixture of phases behind the front); and the solution again has the Lee-Tupper structure $\hat{\mathbf{C}}^{\mathbf{A/M}}\vec{\mathbf{S}}^{\mathbf{c}}\mathbf{C}^{\mathbf{c}}\vec{\mathbf{S}}^{\mathbf{EL}}\mathbf{C}^{\mathbf{A}}_{0}$, where

$$\vec{\mathbf{S}}^{\mathbf{c}} = \vec{\mathbf{S}}[\{e^{M}_{S0}, 0, T_0\} \mathbin{⍓} \{\hat{e}, \hat{x}, \hat{T}\}]$$

The $\vec{\mathbf{S}}^{\mathbf{c}}$-Rayleigh chord begins at the critical point (e^{M}_{S0}, s^{M}_{S0}) of the initial cold isotherm $e = I_L(T_0, s)$ and ends at the point $(\hat{e}, \hat{s})$ of the A/M-branch of the hot isotherm $e = I_L(\hat{T}, s)$ (see Figure 9).

Let us give some estimates for the shock velocity in cases 2 and 3. The phase fraction $\hat{x} = \hat{x}(\hat{s})$ is given implicitly by two equations

$$\hat{x} = Z^{M}(\hat{s}, \hat{T})$$
$$\hat{T} = T_0 \exp(w\hat{x})$$

Since w is of the order of 10^{-1} for SMA materials and $0 < \hat{x} < 1$ we can expand $\hat{T}(w\hat{x})$ in a Taylor series which, along with (2.5,7) and (2.2) results in:

$$\begin{aligned} \hat{x}(\hat{s}) &= a^{M}(\hat{T} - T^{M}_{S}(\hat{s})) = a^{M}\left(T_0(1 + w\hat{x} + O(w\hat{x})^2) - T^{M}_{S}(\hat{s})\right) \\ \hat{e}(\hat{s}) &= \mathrm{K}\hat{s} + n_0(\hat{s} - s^{M}_{S0}) + O\left(w\, l_0^{-1}(\hat{s} - s^{M}_{S0})\right)^2 \end{aligned} \tag{5.14}$$

where $n_0 = \dfrac{awT_0 + \Lambda}{k^{M}(T^{M}_{S0} - T^{M}_{f0} + wT_0)}$. Therefore, disregarding higher order terms we obtain linear relationship for $\hat{x}$:

$$\hat{x}(\hat{s}) = \frac{\hat{s} - s^{M}_{S0}}{k^{M}(T^{M}_{S0} - T^{M}_{f0} + wT_0)} \tag{5.15}$$

for $\hat{s} \in [s^{M}_{S0}, s^{M}_{m0}]$. The isentropic curve $\hat{e}(\hat{s})$ begins at the critical point (e^{M}_{S0}, s^{M}_{S0}) of the cold isotherm $e = I_L(T_0, s)$ and ends at the inner corner point (kink) (e^{M}_{m0}, s^{M}_{m0}) of the hot isotherm $e = I_L(T^{M}_{m0}, s)$. Our calculation shows that the second-order term is at least 10^8 times smaller than the linear term and, for all practical purposes, may be omitted. The curve $\hat{e}(\hat{s})$ is a straight line up to the second order in $w\hat{x}$:

$$\hat{e} = \mathrm{S}_L(T_0, \hat{s}) = \begin{cases} \mathrm{K}\hat{s} & \hat{s} < s^{M}_{S0} \\ (\mathrm{K} + n_0)(\hat{s} - s^{M}_{S0}) + e^{M}_{S0} & s^{M}_{S0} < \hat{s} < s^{M}_{m0} \\ \mathrm{K}\hat{s} + a(T^{M}_{m0} - T_0) + \Lambda & \hat{s} > s^{M}_{m0} \end{cases}. \tag{5.18}$$

Hence, the $\bar{\mathbf{S}}^{\mathbf{c}}$-Rayleigh chord coincides with $\hat{e} = \hat{e}(\hat{s})$ up to the second-order term and the Lee-Tupper solution for the shock isentrope $\hat{e} = \mathsf{S}_L(T_0, \hat{s})$ coincides with the trilinear isentrope $e = E_L(S_0, s)$ to the second order in shock intensity. Therefore, we can now easily evaluate $n(S_0, e)$ from Equation (5.10) as

$$n(S_0, e) \cong n_0 = \frac{awT_0 + \Lambda}{k^M (T_{S0}^M - T_{f0}^M + wT_0)} \cong \frac{\Lambda}{k^M (T_{S0}^M - T_{f0}^M + wT_0)}$$

where $T_0 = T_R \exp((\mathrm{S}_0 - S_R^A)/C)$. Using (5.18) for the shock isentrope and using $e^* = e_{S0}^M$ in (5.10), it is easy to find the velocity of an isentropic phase transformation front.

For $\hat{s} > s_{\mathrm{m}0}^M$, the temperature behind the phase front is independent of $\hat{s}$ and is given by the constant $\hat{T} = T_{\mathrm{m}0}^M$, while the velocity of the phase transformation front is given by

$$D_2^{\mathrm{PT}}\Big|_{S=S_0} = \sqrt{\frac{\hat{s} - s_{\mathrm{S}0}^M}{r(\mathrm{K}\hat{s} + a(T_{\mathrm{m}0}^M - T_0) + \Lambda - e_{\mathrm{S}0}^M)}} \cong \frac{1}{\sqrt{r\left(\mathrm{K} + c(\hat{s})\right)}}. \tag{5.19}$$

The velocity of the phase front depends essentially on the applied stress $\hat{s}$, and is independent of the thermodynamic parameters. In other words, for intense loading ($\hat{s} > s_{\mathrm{m}0}^M$), the latent heat release does not affect the front velocity (up to the small thermoelastic term $a(T_{\mathrm{m}0}^M - T_0)$), and therefore it is approximately the same as the isothermal shock velocity (4.26):

$$D_2^{\mathrm{PT}}\Big|_{S=S_0} \cong\cong D_2^{\mathrm{PT}}\Big|_{T=T_0}.$$

The material velocity behind the phase transformation front can now be found easily using (5.11).

For $s_{S0}^M < \hat{s} < s_{m0}^M$, the velocity of the phase front is given by

$$D_3^{\mathrm{PT}}\Big|_{S=S_0} = \sqrt{\frac{1}{r(\mathrm{K} + n_0)}} \cong \frac{1}{\sqrt{r\left(\mathrm{K} + \left(k^M (T_{S0}^M - T_{f0}^M + wT_0)\right)^{-1}\Lambda\right)}}. \tag{5.20}$$

In this case, the velocity of the phase front is independent of the impact stress $\hat{s}$ and depends only on the mechanical (Λ) and thermodynamic parameters (w) of the phase transformation. It also depends on the initial temperature T_0 and the kinetic parameters k^M, T_{S0}^M and T_{f0}^M. Note that this expression (5.20) gives a lower limit for the velocity of an isentropic phase front of partial transformation for both the Lee-Tupper and Abeyaratne-Knowles solutions. The temperature behind the front is given by (5.14) and depends on the impact stress $\hat{s}$ and on the parameters w and l_0. For NiTi SMA materials (see data in Table 1), the velocity of the phase front is $D_3^{\mathrm{PT}}\Big|_{S=S_0} = 740\mathrm{m/s}$. Note that the front velocity is higher in the isentropic case than in the isothermal case:

$$D_3^{\mathrm{PT}}\Big|_{S=S_0} > D_3^{\mathrm{PT}}\Big|_{T=T_0}.$$

5.2 Numerical results. As an example to the theory developed in this section we used the Lax-Fridriechs scheme to solve the adiabatic shock-loading problem (2.1),(3.2) and (3.5) along with the initial and boundary conditions (5.2). The three field varibales - strain $e(x,t)$, velocity $\mathrm{v}(x,t)$ and temperature $\mathrm{T}(x,t)$ were discretized in the same manner as in section 4.3. The material parameters used are the one shown in Table 1 and the applied stress was $\hat{s} = 600MPa$. This stress level was sufficient to induce almost full transformation ($x \cong 0.99$ in the transformed region of the rod) so we are in the case $s_{S0}^M < \hat{s} < s_{m0}^M$. As in the isothermal case, the finite difference solution is the Lee-Tupper solution with a corner shock. The strain profile at t=10ms is given on Figure 11 while the profile of the martensitic volume fraction and temperature are given on Figures 12 and 13, respectively. The numerical value for the velocity of the phase front is $\cong 810\mathrm{m/s}$ which is within 10% of the analytical value for D_3^{PT}. This result comes to illustrate the fact that the isentropic approximation (3.11) that we used to obtain analytical results is close enough to the adiabatic one (3.5).

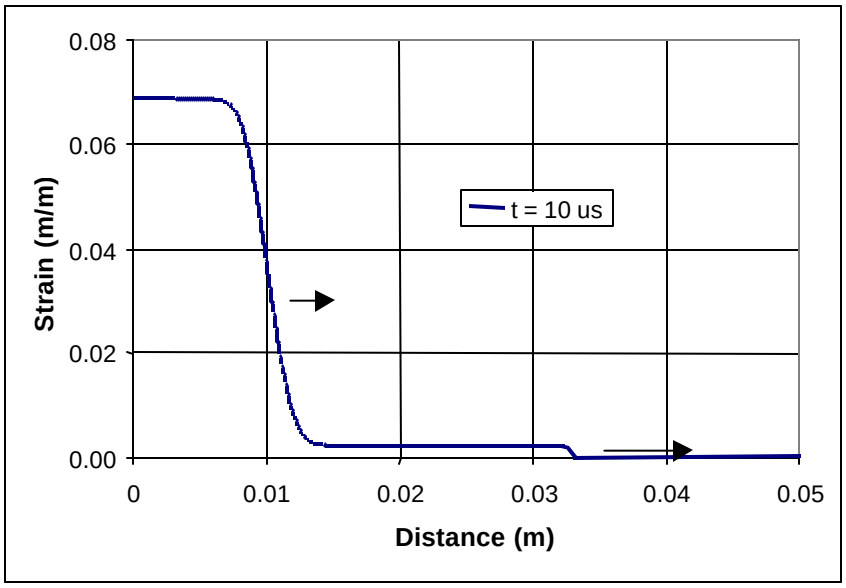

Figure 11. Numerical Strain profile for the SMA adiabatic impact problem: $\hat{s}$ = 600 MPa **(Lax-Friedrichs scheme)**

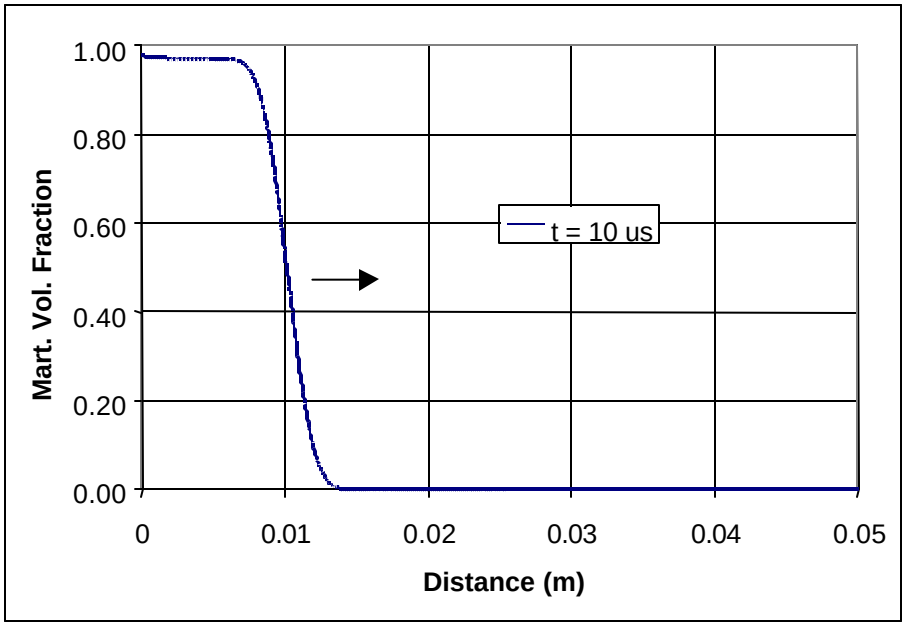

Figure 12. Numerical martensite fraction profile for SMA adiabatic impact problem: $\hat{s}$ = 600 MPa **(Lax-Friedrichs scheme)**

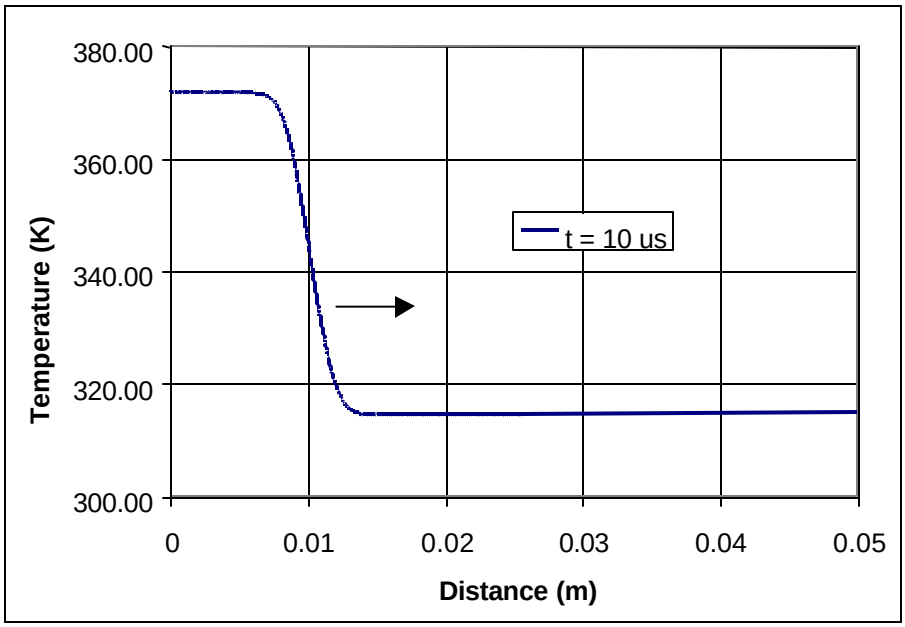

Figure 13. Numerical temperature profile for SMA adiabatic impact problem: $\hat{s} = 600$ MPa **(Lax-Friedrichs scheme)**

SUMMARY AND CONCLUSIONS

In this paper we developed the solution to the impact loading problem for an SMA rod in an isothermal and adiabatic setting. Several different kinetic laws were considered and a well-defined transformation front was found for each one of them. Analytical expressions for the velocity of phase transformation front were obtained. It was found that without additional thermodynamic assumptions (e.g. [44]) non-unique solutions are possible. Numerical examples were presented based on Lax-Friedrichs finite difference scheme for both the isothermal and adiabatic cases. It was found that this numerical approach renders a unique solution due to the numerical viscosity introduced by the solver. Results from these numerical solutions were found to be in very good agreement with the predicted analytical solutions.

ACKNOWLEDGMENTS

The support of the Office of Naval Research, grant No. N00014-97-1-0943 (Dr. Allen Moshfegh, program monitor) as well as the support of Air Force Office of

Scientific Research, grant No. F49620-01-1-0196 (Dr. Dan Segalman, program monitor) is greatly appreciated.

REFERENCES.

[1] Tanaka, K. A thermomechanical sketch of shape memory effect: One dimensional tensile behavior. Res Mech., 18, 251-263 (1986).

[2] Tanaka, K. A phenomenological description on thermomechanical behavior of shape memory alloys. Trans. ASME Journal of Pres. Ves. Tech., 112, 158-163 (1990).

[3] Bekker, A. (1997). Mathematical Modeling of One Dimensional Shape Memory Alloy Behavior. Ph. D. Thesis, Northwestern University. Evanston, IL.

[4] Bekker, A. and C. Brinson. Phase diagram based description of hysteresis behavior of shape memory alloys. Acta Mater., 10, 3649-3665 (1998).

[5] Bekker, A. and L. C. Brinson. Thermo-induced transformation in a prestressed 1-D SMA polycrystalline body: Phase diagram kinetics approach. J. Mech. Phys. Solids, 45, 949-988 (1997).

[6] Boyd, J. G. and D. C. Lagoudas. A thermodynamic constitutive model for the shape memory materials. Part I. The monolithic shape memory alloys. Int. J. Plasticity, 12, 805-841 (1996).

[7] James, R. D. The propagation of phase boundaries in elastic bars. Arch. Rational Mech. Anal., 73, 125-158 (1980).

[8] Pence, T. J. On the emergence and propagation of a phase boundary in a elastic bar with a suddenly applied end load. J. Elast., 16, 3-42 (1992).

[9] Abeyaratne, R. and J. K. Knowles: Dynamics of propagating phase boundaries: adiabatic theory for thermoelastic solids. Physica D, 79, 269-288 (1994).

[10] Abeyaratne, R. and J. K. Knowles: Dynamics of propagating phase boundaries: Thermoelastic solids with heat conduction. Arch. Rational Mech. Anal., 126, 203-230 (1994).

[11] Abeyaratne, R. and J. K. Knowles: Impact-induced phase transitions in thermoelastic solids. Phil. Trans. R. Soc. Lond. A, 355, 843-867 (1997).

[12] Truskinovsky, L. Transition to detonation in dynamic phase changes. Arch. Rational Mech. Anal., 125, 375-397 (1994).

[13] Truskinovsky, L. About the normal growth approximation in the dynamic theory of phase transitions. Cont. Mechanics and Thermodynamics, 6, 185-208 (1994).

[14] Kuzina, Z. N. et al. Nonlinear waves in a viscoelastic rod and the problem of impact of a finite rod on a rigid obstacle. Zh. Prikl. Mekh. Tekh. Fiz., (1), 143-153 (1978).

[15] Leonov, A. I. Nonisothermal nonlinear waves in a rod made of a dissipative rubberlike material. Zh. Prikl. Mekh. Tekh. Fiz., (3), 135-145 (1978).

[16] Al'tshuler, L. V. Use of shock waves in high-pressure physics.” Sov. Phys. - Usp., 8(1), 52-91 (1965).

[17] Al'tshuler, L. V. Phase transitions in shock waves (Review). Zh. Prikl. Mech. Tech. Fiz., 4, 93-103 (1978).

[18] Duvall, G. E. and R. A. Graham. Phase transitions under shock-wave loading. Rev. Mod. Phys., 49 (3), 523-579 (1977).

[19] Menikoff, R. and B. J. Plohr. The Riemann problem for fluid flow of real materials. Rev. Mod. Phys., 62(1), 75-130 (1989).

[20] Courant, R. and K. O. Friedrichs. Supersonic Flow and Shock Waves, Springer-Verlag, New York, 1948.

[21] Kestin, J. Metal plasticity as a problem in thermodynamics, in Thermomechanical couplings in solids H. D. Bui and Q. S. Nguyen. (North-Holland), Elsevier (1987).

[22] Maugin, G. A. and W. Muschik. Thermodynamics with internal variables; Part I: General concepts. J. Non-Equilib. Thermodyn., 19, 217-249 (1994).

[23] Lagoudas, D. C., et al. A unified thermodynamic constitutive model for SMA and finite element analysis of active metal matrix composites. Mech. Comp. Matls. Struct., 8, 153-179 (1996).

[24]Paskal, Y. I. and L. A. Monasevich. Hysteresis features of the martensitic transformation of titanium nickelide. Phys. Met. Metall., 52(5), 95-99 (1981).

[25] Bondaryev, E. N. and C. M. Wayman. Some stress-strain-temperature relationships for shape memory alloys. Metall. Trans. A, 19A, 2407-2413 (1987).

[26] Sun, Q. P. and K. C. Hwang. Micromechanics modeling for the constitutive behavior of polycrystalline shape memory alloys - 1,2. J. Mech. Phys. Solids, 41(1), 1-17 (1993).

[27] Cory, J. S. and J. L. McNichols. Nonequilibrium thermostatics. J. Appl. Phys., 58, 3282-3294 (1985).

[28] McNichols, J. L. and J. S. Cory. Thermodynamics of Nitinol. J. Appl. Phys., 61, 972-984 (1987).

[29] Kulikovskii, A. and E. Sveshnikova. Nonlinear Waves in Elastic Media, CRC Press, New York, 1995.

[30] Wallace, D. C. Equation of state from weak shocks in solids." Phys. Rev. B, 22(4), 1495-1502 (1980).

[31] Karman, T. and P. Duwez. The propagation of plastic deformation in solids. J. Appl. Phys., 21, 987-994 (1950).

[32] Barenblatt, G. I. On the propagation of instantaneous excitations in media with nonlinear stress-deformation relation. Prikl. Mat. Mekh., 17, 455-460 (1953).

[33] Barenblatt, G. I. (1979). Similarity, Self-Similarity and Intermediate Asymptotics. New York, Consultant Bureau.

[34] Bethe, H. A. (1942). The theory of shock waves for an arbitrary equation of state. Report No. PB-32189 (Clearing House for Sci. and Tech. Information). Washington, D.C., U. S. Department of Commerce.

[35] Gelfand, I. M. (1959). Some Problems in the Theory of Quasi-linear Equations. Usp. Mat. Nauk, 14.

[36] Wendroff, B. The Riemann problem for materials with nonconvex equations of state: I Isentropic flow. J. Math. Anal. Appl., 38, 454-466 (1972).

[37] Isaacson, E. L. et al. Transitional waves for conservation laws. SIAM J. Math. Anal., 21, 837-866 (1990).

[38] Smith, J. F., et al. C_p and fractal phase transformation in the shape memory alloy Ni-52Ti. Mater. Sci. Eng., A149, 11-120 (1991).

[39] Abeyaratne, R. and J. K. Knowles: On the driving traction acting on a surface of strain discontinuity in a continuum. J. Mech. Phys. Solids, 38, 345-360 (1990).

[40] Abeyaratne, R. and J. K. Knowles: Kinetic relations and the propagation of phase boundaries in solids. Arch. Rational Mech. Anal., 114, 119-154 (1991).

[41] Rosakis, P. An equal area rule for dissipative kinetics of propagating strain discontinuities. SIAM J. Appl. Math., 55, 100-123 (1995).

[42] Abeyaratne, R. and J. K. Knowles: On the propagation of maximally dissipative phase boundaries in solids. Quart. Appl. Math., L, 149-172 (1992).

[43] Truskinovsky, L. Kinks versus shocks, in Shock Induced Transitions and Phase Structures in General Media, pp. 187-229, ed., J. E. Dunn, R. Fosdick and M. Slemrod, Springer-Verlag**,** New York**,** 1993.

[44] Chen, Y. C. and D. C. Lagoudas (1999). Impact induced phase transformation in shape memory alloys. Journal of Mechanical Physics Solids., 48, 275-300 (2000).

[45] Lax, P. D.. Weak solutions of nonlinear hyperbolic equations and their numerical computation. Comm. Pure Appl. Math., 7, 159-193 (1954).

[46] Lee, E. H. and S. J. Tupper. Analysis of plastic deformation in a steel cylinder striking a rigid target. J. Appl. Mech., 21, 63-70 (1954).

[47] Bancroft, D. et al. Polymorphism of iron at high pressure. J. Appl. Phys., 27 (3), 291-298 (1956).

[48] Cramer, M. S. and R. Sen. Exact solutions for sonic shocks in van der Waals gases. Phys. Fluids, 30 (2), 377-385 (1987).

[49] Cramer, M. S.. Shock splitting in single-phase gases. J. Fluid Mech., 199, 281-296 (1989).

[50] Wright, T. W. Axial plastic waves waves in a rod. Studies in Appl. Math., 72, 149-160 (1985).

[51] Whitham, G. B. Linear and Nonlinear Waves, John Wiley & Sons, New York, 1974.

[52] Qidwai, M.A and D.C. Lagoudas. Numerical implementation of a shape memory alloy thermomechanical constitutive model using return mapping algorithms. Int. J. Numer. Meth. Engng., 47, 1123-1168 (2000).

[53] Graff, K.F. Wave Motion in Elastic Solids, Oxford University Press, London, 1975

[54] Malvern, L.E, Introduction to the Mechanics of a Continuous Medium, Prentice-Hall Inc., Englewood Cliffs, N.J., 1977

[55] Abeyaratne, R., Knowles J.K., On a shock-induced martensitic phase transition, J. Appl. Phys., 87 (3), 1123-1134, (2000).

[56] Bekker, A., Jimenez-Victory, J.C., Lagoudas, D.C. Shock Propagation of Phase Transitions in SMA Rods, Technical Report No. CMC-2001-01, Center for Mechanics of Composites, Texas A&M University, 2001.

[57] Qidwai, M.A., Lagoudas, D.C. On thermomechanics and transformation surfaces of polycrystalline NiTi shape memory alloy material, Int. J. Plasticity 16 (10-11) (2000) pp. 1371-1390

[58] Gao, X., Huang, M., Brinson, L.C. A multivariant micromechanical model for SMAs Part 1. Crystallographic issues for single crystal model. Int. J. Plasticity 16 (10-11) (2000) pp. 1345-1369

[59] Gao, X., Huang, M., Brinson, L.C. A multivariant micromechanical model for SMAs Part 2. Polycrystal model. Int. J. Plasticity 16 (10-11) (2000) pp. 1371-1390

[60] Sittner, P., Novak, V., Anisotropy of martensitic transformations in modeling of shape memory alloy polycrystals. Int. J. Plasticity 16 (10-11) (2000) pp. 1243-1268

[61] Gall, K., Lim, J., McDowell, D., Sehitoglu, H., Chumlyakov, Y. The role of intergranular constraint on the stress-induced martensitic transformations in textured polycrystalline NiTi. Int. J. Plasticity 16 (10-11) (2000) pp. 1189-1214

[62] Huang M., Brinson L.C. A Multivariant model for single crystal shape memory alloy behavior. J. Mech. Phys. Solids 46 (8), 1379-1409.

[63] Kitajima, Y., Sato N., Tanaka, K., Nagaki, S. Crystal-based simulations in transformation thermomechanics of Shape Memory Alloys, *in print* Int. J. Plasticity (2002)

[64] Patoor, E., Barbe, P., Eberhard, A. and Berveiller, M. Thermomechanical Behaviour of Shape Memory Alloys. Arch. Mech. 40, 775—794

[65] Tokuda, M., Ye, M., Takakura, M., Sittner, P. Calculation of mechanical behaviors of shape memory alloy under multiaxial loading conditions, International Journal of Mechanical Sciences 40(2-3) 227-235

[66] Levitas, V. Critical thought experiment to choose the driving force for interface propagation in inelastic materials. *in print* Int. J. Plasticity (2002)